Shipboard Landing Control Enabled by an Uncertainty and Disturbance Estimator

Qi Lu,* Beibei Ren,† and Siva Parameswaran‡
Texas Tech University, Lubbock, Texas 79409

DOI: 10.2514/1.G003073

This paper presents an autonomous landing control approach for a quadrotor unmanned aerial vehicle subject to wind disturbance and three-dimensional movements of the landing platform. To achieve an accurate relative position estimation of the quadrotor to the landing platform, a camera, a distance sensor, and a single-board computer are integrated to the quadrotor. The coordinate transformation is introduced to deal with the constraint that only the relative position information is available. The impacts of unknown ship motions are treated as part of the lumped uncertainty terms. Then, the uncertainty and disturbance estimator-based controllers are developed to achieve the accurate relative position control of the quadrotor while dealing with unknown ship motions, ground effect, state couplings, and external disturbances. The uncertainty and disturbance estimator filter is designed based on the internal model principle to enhance the performance of the developed controller. The reference model of the relative altitude controller is modified to ensure the accurate tracking of descending commands. To maximize the capability of the developed controller, a parameter selection guideline based on the derived ship heave acceleration spectrum is provided. Both numerical simulations and flight experiments are carried out to demonstrate the effectiveness of the developed approach.

Nomenclature

A_z, B_z, χ_z	=	state matrix, input matrix and state vector for Δz dynamics, respectively
b	=	thrust force input coefficient
e_x, e_y, e_z	=	closed-loop system tracking error vectors for Δx, Δy, and Δz dynamics, respectively
F	=	total thrust force generated by rotors in $\mathcal{Q}$, N
g	=	gravitational acceleration, $9.8\,\mathrm{m/s^2}$
$I = \begin{bmatrix} I_{xx} & 0 & 0 \\ 0 & I_{yy} & 0 \\ 0 & 0 & I_{zz} \end{bmatrix}$	=	quadrotor body inertia matrix, $\mathrm{kg \cdot m^2}$
$\mathcal{I} = \{\boldsymbol{x}_I, \boldsymbol{y}_I, \boldsymbol{z}_I\}$	=	inertia frame
k_F	=	rotor thrust coefficient, $\mathrm{N/rpm^2}$
k_M	=	rotor drag coefficient, $(\mathrm{N \cdot m})/\mathrm{rpm^2}$
k_m	=	motor bandwidth, $\mathrm{s^{-1}}$
l	=	arm length, m
m	=	quadrotor mass, kg
$\mathcal{Q} = \{\boldsymbol{x}_Q, \boldsymbol{y}_Q, \boldsymbol{z}_Q\}$	=	quadrotor body frame
R	=	radius of the propeller, m
$\mathcal{S} = \{\boldsymbol{x}_S, \boldsymbol{y}_S, \boldsymbol{z}_S\}$	=	ship body frame
$S, S_E, S_R, S_{\mathrm{ACC}}$	=	sea wave, ship encounter wave, ship heave motion, and ship heave acceleration spectrums, respectively, $\mathrm{m^2 \cdot s}$
U_0	=	ship forward speed, m/s
$u_\xi = [\,u_x \quad u_y \quad u_z\,]^T$	=	control inputs for the relative position dynamics
x_r, y_r, z_r	=	calculated quadrotor position references in $\mathcal{I}$, m
z_R	=	average height of the quadrotor propellers in $\mathcal{I}$, m
Γ	=	encounter angle, deg
$\Delta\xi = [\,\Delta x \quad \Delta y \quad \Delta z\,]^T$	=	relative positions, m
$\Delta\xi_r = [\,\Delta x_r \quad \Delta y_r \quad \Delta z_r\,]^T$	=	relative position references, m
$\Delta\psi, \Delta\psi_r$	=	relative yaw and relative yaw reference, respectively
$\eta = [\,\phi \quad \theta \quad \psi\,]^T$	=	quadrotor Euler angles, deg
$\nu = [\,\dot{x} \quad \dot{y} \quad \dot{z}\,]^T$	=	quadrotor translational velocities in $\mathcal{I}$, m/s
$\xi = [\,x \quad y \quad z\,]^T$	=	quadrotor positions in $\mathcal{I}$, m
$\xi_s = [\,x_s \quad y_s \quad z_s\,]^T$	=	ship positions in $\mathcal{I}$, m
$\tau = [\,\tau_\phi \quad \tau_\theta \quad \tau_\psi\,]^T$	=	torques along quadrotor body axes, $\mathrm{N \cdot m}$
$\chi_{mx}, \chi_{my}, \chi_{mz}$	=	state vectors of the reference models for Δx, Δy, and Δz dynamics, respectively
χ_{mz1}	=	first component of the vector χ_{mz}, m
$\Omega = [\,p \quad q \quad r\,]^T$	=	quadrotor rotational velocities in $\mathcal{Q}$, deg/s
ω_w, ω_E	=	sea wave and encounter wave frequencies, respectively, rad/s
$\omega_{0R}, \omega_{0\mathrm{ACC}}$	=	peak frequencies of the ship heave motion and ship heave acceleration spectrums, respectively, rad/s

Received 20 May 2017; revision received 31 December 2017; accepted for publication 7 January 2018; published online 28 February 2018.

*Ph.D. Student, Department of Mechanical Engineering; qi.lu@ttu.edu.
†Assistant Professor, Department of Mechanical Engineering; beibei.ren@ttu.edu.
‡Professor, Department of Mechanical Engineering; siva.parameswaran@ttu.edu.

I. Introduction

THE research in the automation of unmanned aerial vehicles (UAVs) has evolved rapidly over the past decades, which is driven by their various applications ranging from military combat to civilian infrastructure inspection [1,2]. Moreover, compared to manned aircrafts, the UAVs are more suitable and expandable for dull, dirty, and dangerous missions [3]. The use of UAVs in open seas provides the convenience for operators to conduct efficient maritime operations, such as offshore wind-turbine monitoring and ocean surveying. To be applicable in maritime applications, it requires the UAVs to autonomously take off and land on moving platforms, such as the ship deck or the landing pad attached to a vessel [4]. Compared with other phases during the autonomous operation of the UAVs, landing is probably the most intricate and challenging component.

About 50% of fixed-wing UAVs suffer accidents during landing, and almost 70% of mishaps are caused by human factors [5]. Therefore, to alleviate the pilot's load and achieve safe landing, the study of autonomous shipboard landing control for UAVs posses both theoretical and practical importance. Among all kinds of UAVs, the quadrotor has the attracting features of low cost, easy deployment, and vertical takeoff and landing ability [6,7]. It is adopted as the validation platform in this work.

The navigation and control are two essential parts to achieve accurate and safe shipboard landing. A typical navigation system for shipboard landing uses the fused measurements from GPS and the inertial measurement unit (IMU) to provide the position information of the UAV and the ship deck [8]. However, the accuracy of GPS is usually around several meters [9]. To enhance the performance of the GPS system, the differential GPS and the real-time kinematic algorithms are used [10]. Nevertheless, the accessibility of GPS signal is subject to satellite availability, signal blockage from the ship's superstructure, jamming, and spoofing [11,12]. Instead of relying on traditional GPS-based navigation methods, recent studies have also investigated the tether-based [13,14], infrared feature-based [15], optical flow-based [4], and marker-based [16,17] approaches to provide the localization information during UAV landing. In [16,17], the ArUco marker and AprilTags are used to provide the position estimation of the landing platform. The localization method based on the ArUco library [18] provides drift-free estimation of the marker position and orientation. Additionally, the generation and preparation of the ArUco marker are relatively simple, and there are no special requirements for the camera. Therefore, in this paper, the relative navigation information is provided by a TeraRanger One distance sensor [19] and a camera, which is used for marker detection.

The landing operation usually consists of several phases [20]. In this paper, the landing process is divided into three phases. The first phase is the lock-in phase, where the quadrotor is commanded to hover above the moving ship. After synchronization between the quadrotor and the ship is achieved, the second phase (descending) will be started by controlling the quadrotor to follow the predefined descending path. When the quadrotor is close enough to the landing platform, the final phase (touchdown) is initiated by decreasing the thrust at a constant rate. For the selection of the landing trajectory, in [21], a smooth sigmoid function is used as the reference path to achieve the smooth landing. The reference path in [4] is an exponential function, which is specified by the desired optical-flow divergence. A trajectory generation module is used in [22] to generate the time-optimal landing trajectory. In [17], a ramp reference signal with constant descent rate is used to achieve quick and safe descent. The parameterization of a ramp signal is relatively simple, and it is computationally efficient, making it suitable for the implementation on the flight control board of the quadrotor, where computational power is limited. Thus, in this paper, the descending path is chosen as a ramp signal.

As for the control algorithm development, there exist a number of challenges due to the nonlinear dynamics of the quadrotor and the complex maritime environment. First, the quadrotor is a naturally unstable system with coupled states [23]. Moreover, the ground effect when the quadrotor flying proximity to the landing platform causes the rotors to generate additional nonlinear lifting forces, making the controller hard to stabilize [16,22]. Second, the battery voltage dropping/fuel consumption and payload change lead to time-varying model uncertainties. Third, the landing platform (ship deck) is in random heave motion due to the interaction with the sea wave. To avoid collision and achieve safe landing, the ship deck motions should be taken into consideration when designing the controller. Moreover, the accurate motion information of the ship and the quadrotor in the inertia frame is hard to measure. The problem becomes particularly challenging when solely the relative position information is available. To achieve synchronization between the quadrotor and the landing platform, the controller's task is to force the quadrotor to track a time-varying reference trajectory whose information is not readily available [24]. Fourth, the wind gust from the environment and air wakes generated by the ship superstructure, which are acting as external disturbances, cause problems for safe and accurate landing operations.

To deal with the preceding challenges, various control methods have been proposed. The classical proportional–integral–derivative controller possesses the merits of easy implementation and computational efficiency. Therefore, it has been widely adopted for the control execution to achieve safe landing [11,16,17]. However, without considering the system nonlinearities of the quadrotor and the landing platform motion, such methods may lead to suboptimal performance [8]. As for the treatment of random ship motion, which is the major challenge of the shipboard landing control, the existing methods can be categorized into two camps. The first category of method constructs the ship motion estimator to provide the ship deck motion information through the fusion of measurements from the vision system, IMU, and GPS [22,25]. For instance, in [22], a motion estimation module based on an unscented Kalman filter is constructed. Then, the estimated ship deck motion is fed to the developed adaptive robust controller. In [25], a modified Prony analysis procedure is used to estimate the mean ship deck height. Nevertheless, the ship motion estimator requires substantial time to initialize [21], and the motion control accuracy is also dependent on the performance of the ship motion estimator [4]. This motivates researchers to investigate the second category of estimator-free methods, where the effects of the random ship motions are treated as disturbances. In [21], an altitude controller for a quadrotor based on the invariant ellipsoid technique is developed to handle the ship heave motion. The optimal control gain is computed to achieve the minimum ellipsoid size, which is also the error response bound. The time delay control (TDC) augmented proportional-derivative controller is investigated in [20] for a helicopter to achieve the autonomous shipboard landing mission, where the TDC is designed to compensate the effects of ship motions, model uncertainties, and crosswinds. In [26], a disturbance estimator for constant, or slowly time-varying, unknown inertial forces, which are generated from the motion of the landing platform, is included in the control law to improve its performance. The control algorithm based on the internal model principle along with the frequency adaptation law is developed in [24] to account for the effect of the ship deck oscillations. In this paper, for the treatment of the random ship motion, the latter approach is adopted by regarding the impacts of the ship motion as part of the lumped uncertainty terms. The coordinate transformation is introduced to solve the sensing limitations where solely the relative navigation information is available. Then, the uncertainty and disturbance estimator (UDE) based position controllers are developed in the relative coordinates to handle the influence of unknown ship motions, state couplings, ground effect, model uncertainties, and external disturbances. The UDE-based control method was proposed in [27], whose basic idea is that, in the frequency domain, an engineering signal can be approximated by putting it through a filter with the appropriate bandwidth. In recent years, the remarkable performance of the UDE strategy has been validated through various applications, such as servomotor [28,29], variable-speed wind turbine [30], power system [31,32], and UAV [33–35].

Compared with the existing approaches proposed in the literature, the developed approach has several aspects of advantages. First, because the proposed approach is derived in relative coordinates, it is suitable for the scenarios where only the measurements from the onboard sensors are available (e.g., the GPS-denied environment). Second, the ship motion estimation module is not required, making the developed UDE-based controller have a relatively simple structure and easier implementation. Third, the robustness and performance of the developed UDE-based controller are further improved with the UDE filter, which is designed based on the internal model principle, the modified reference model, and the derived controller parameter selection guideline from the analysis of the derived ship heave acceleration spectrum. The limitation of the developed method lies in the requirement of the sea state data, which may be available from the marine weather forecasts. Additionally, as a visual-based method, adequate lighting is needed to provide reliable navigation information. The artificial marker should also be placed on the landing platform before the initiation of the landing operation.

The contributions of this paper are summarized as follows.

To achieve accurate relative navigation between the quadrotor and landing platform, a camera, a TeraRanger One distance sensor, and an Odroid XU4 single-board computer are integrated. The marker design, which consists of two concentric ArUco markers with different sizes, is used to ensure the localization data available during the whole landing process from high altitude to low altitude. To deal with the limitations where solely the relative navigation information is available, the coordinate transformation is introduced. Then, the UDE-based position controllers are developed in the relative coordinates and applied to the quadrotor autonomous landing operation. To deal with the random ship heave motion, the UDE filter is designed based on the internal model principle with the guideline provided in [29]. The parameter selection guideline from the analysis of the derived ship heave acceleration spectrum is developed to maximize the capability of the developed controller. Moreover, the reference model is modified to enhance the tracking performance of the developed controller. The detailed stability analysis of the closed-loop system and performance analysis of the reference model are provided. Simulation studies are carried out to validate the effectiveness of proposed approach with the ship motion simulated based on the sea wave spectrum, realistic sea state data, and response amplitude operator (RAO) data from the literature. Furthermore, extensive flight experiments are carried out with the self-built quadrotor platform and the self-built landing platform in a laboratory setup to demonstrate the performance of the developed approach. Even with the presence of wind disturbance and unknown three-dimensional landing platform motions, the autonomous landing is successfully achieved. To the authors' best knowledge, this is the first time that a UDE-based controller with the filter designed based on the internal model principle has been applied to the quadrotor landing control problem and implemented in both simulation and experimental studies.

The rest of this paper evolves along this line. In Sec. II, the mathematical models of the quadrotor and ship motions are presented with the control problem formulated. The details of the UDE-based controller design are discussed in Sec. III. Section IV shows the stability of the closed-loop system and performance analysis of the proposed controller. Simulation studies and flight experiments are carried out in Sec. V to demonstrate the effectiveness of the proposed approach. Conclusions are made in Sec. VI.

II. System Modeling and Problem Formulation

In this section, the modelings of the quadrotor motion and the ship motion in seaway are presented. Based on the developed quadrotor and ship motion models, the relative position dynamics is derived with the coordinate transformation introduced. Then, the control problem for the landing operation is formulated as a relative trajectory tracking problem.

A. Quadrotor System Modeling

The coordinate systems of the inertia frame, the quadrotor body frame, and the ship body frame are illustrated in Fig. 1. Let $\mathcal{I} = \{\boldsymbol{x}_I, \boldsymbol{y}_I, \boldsymbol{z}_I\}$ denote the right-hand inertial frame, with $\boldsymbol{z}_I$ being the vertical direction unit vector pointing toward the ground. The quadrotor body frame $\mathcal{Q} = \{\boldsymbol{x}_Q, \boldsymbol{y}_Q, \boldsymbol{z}_Q\}$ is rigidly attached to the center of gravity of the quadrotor. The ship body fixed frame is denoted by $\mathcal{S} = \{\boldsymbol{x}_S, \boldsymbol{y}_S, \boldsymbol{z}_S\}$, which is attached to the center of gravity of the ship. Let F denote the total lift force, and $\tau = [\tau_\phi \quad \tau_\theta \quad \tau_\psi]^T$ denote the vector consisting of torques along the quadrotor body axes. The positions and translational velocities of the quadrotor with respect to the inertial frame $\mathcal{I}$ are represented by $\xi = [x \quad y \quad z]^T$ and $\nu = [\dot{x} \quad \dot{y} \quad \dot{z}]^T$, respectively. Let $\eta = [\phi \quad \theta \quad \psi]^T$ and $\Omega = [p \quad q \quad r]^T$ denote the Euler angles and angular velocities of the quadrotor, respectively. The rotation matrix $\mathcal{R}$ is used to describe the orientation of the quadrotor. Then, the model of the quadrotor dynamics is represented using the following equations [4]:

$$\dot{\mathcal{R}} = \Omega_\times \mathcal{R} \tag{1}$$

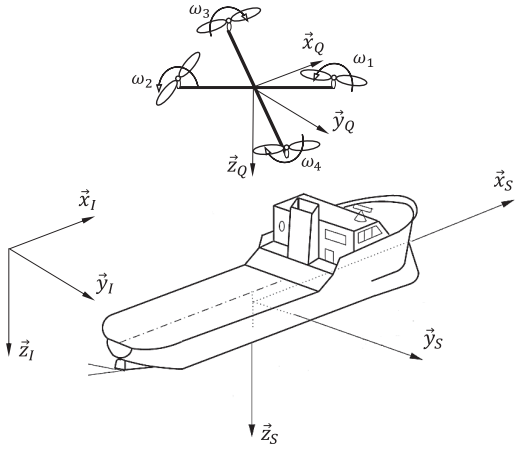

Fig. 1 Coordinate systems for the quadrotor shipboard landing.

$$I\dot{\Omega} = \tau - \Omega_\times I\Omega \tag{2}$$

$$\dot{\xi} = \nu \tag{3}$$

$$m\dot{\nu} = -bF\mathcal{R}z_I + mgz_I \tag{4}$$

where m is the mass; g is the gravitational acceleration; b is the input coefficient; $z_I = [0 \quad 0 \quad 1]^T$ is the vertical unit vector of the inertia frame; I represents the quadrotor body inertia matrix; and $\Omega_\times$ is a skew-symmetric matrix in the form of

$$\Omega_\times = \begin{bmatrix} 0 & -r & q \\ r & 0 & -p \\ -q & p & 0 \end{bmatrix}$$

Let $\xi_s = [x_s \quad y_s \quad z_s]^T$ be the positions of the ship in the inertia frame $\mathcal{I}$. Because of the ground effect, the rotors will gain additional nonlinear lift forces when flying proximity to the landing platform. The input coefficient b, which models the ground effect, can be expressed as [22,36]

$$b = \frac{1}{1 - (R^2/16(z_R - z_s)^2)} \tag{5}$$

where R is the radius of the quadrotor propeller, and z_R is the average height of the four quadrotor propellers in the inertia frame.

Assumption 1: For very small values of $(z_R - z_s)/R$, there exist large errors in Eq. (5) [36]. It is assumed that $(z_R - z_s/R) \geq 0.5$, such that the ground effect model [Eq. (5)] is valid.

Because of the heights of the quadrotor frame, landing gear, and motors, the preceding assumption could be easily satisfied.

B. Ship Motion Modeling

Assumption 2: For the translational motions of the ship, it is assumed that the ship is moving with a constant forward speed (i.e., $\dot{x}_s$ and $\dot{y}_s$ are constants).

The ship heave motion z_s is mainly caused by the interaction with the sea waves [37]. For the simulation of the ship heave motion in seaway, the International Towing Tank Conference (ITTC) sea wave power spectrum $S(\omega_w)$ is recommended [38,39]:

$$S(\omega_w) = 173H_s^2T_1^{-4}\omega_w^{-5}\exp(-691T_1^{-4}\omega_w^{-4}) \tag{6}$$

where $\exp(\cdot)$ is the exponential function, ω_w is the wave frequency, H_s is the significant wave height, and T_1 is the mean wave period. Because the ship is moving with respect to the inertia frame, the sea wave observed from the ship is affected by a Doppler shift [40]. Considering the ship, which is moving with a forward speed U_0 and an encounter angle Γ, which is defined as the angle between the sea

wave propagation direction and the ship heading, the encounter wave spectrum S_E is given by

$$S_E(\omega_E) = \frac{S(\omega_w)}{|1 - (2\omega_w U_0/g)\cos\Gamma|}$$

where ω_E is the encounter wave frequency. With the response amplitudes specified by the RAO [41], the ship heave motion power spectrum can be calculated as

$$S_R(\omega_E) = R_A^2(\omega_E) S_E \tag{7}$$

where R_A is the response amplitude of the ship to the wave excitation. The ship heave motion model is given as the finite sum of sinusoidal components [40]

$$z_s = \sum_{i=1}^{n} M_i \sin(\omega_{Ei} t + \varphi_i) \tag{8}$$

where M_i, ω_{Ei}, and φ_i are amplitude, frequency, and random initial phase of the ith component, respectively. The amplitude M_i for a given frequency ω_{Ei} can be calculated from the ship heave motion spectrum [Eq. (7)] using

$$M_i = \sqrt{2 S_R(\omega_{Ei}) \Delta\omega_E} \tag{9}$$

where $\Delta\omega_E$ is the differential step between successive encounter frequencies.

C. Problem Formulation

Considering the bounded external disturbances d_x and d_y acting on the horizontal dynamics of the quadrotor, the position dynamics of the quadrotor [Eq. (4)] can be rewritten as [34]

$$\ddot{x} = -\frac{b}{m} F[\cos(\psi)\sin(\theta)\cos(\phi) + \sin(\psi)\sin(\phi)] + d_x \tag{10}$$

$$\ddot{y} = -\frac{b}{m} F[\sin(\psi)\sin(\theta)\cos(\phi) - \cos(\psi)\sin(\phi)] + d_y \tag{11}$$

$$\ddot{z} = -\frac{b}{m} F[\cos(\theta)\cos(\phi)] + g \tag{12}$$

Assumption 3: It is assumed that the heading angle ψ will be first controlled to be aligned with the heading of the ship before the quadrotor starts landing.

The virtual controls for quadrotor horizontal dynamics are designed as [34]

$$\begin{aligned} u_x &= \theta_r \cos(\phi) \\ u_y &= -\phi_r \end{aligned} \tag{13}$$

by approximating $\sin(\theta_r)$ and $\sin(\phi_r)$ as θ_r and ϕ_r. Choosing the control input for the altitude dynamics as $u_z = g - (F/m)$ and defining the relative coordinates as $\Delta\xi = [\,\Delta x \quad \Delta y \quad \Delta z\,]^T = \xi - \xi_s$, the relative system dynamics can be written as

$$\begin{aligned} \Delta\dot{\xi} &= \dot{\xi} - \dot{\xi}_s \\ \Delta\ddot{\xi} &= B u_\xi + D \end{aligned} \tag{14}$$

where $u_\xi = [\,u_x \quad u_y \quad u_z\,]^T$ is the control input vector, $B = [-(F/m) \;\; -(F/m) \;\; 1]$ is the input matrix, and $D = [D_x \;\; D_y \;\; D_z]^T$ represents the vector of lumped uncertainty terms in the form of

$$\begin{aligned} D_x &= -\frac{F}{m}[b\cos(\psi)\sin(\theta)\cos(\phi) + b\sin(\psi)\sin(\phi) - u_x] - \ddot{x}_s + d_x \\ D_y &= -\frac{F}{m}[b\sin(\psi)\sin(\theta)\cos(\phi) - b\cos(\psi)\sin(\phi) - u_y] - \ddot{y}_s + d_y \\ D_z &= -\frac{F}{m}[b\cos(\theta)\cos(\phi) - 1] - \ddot{z}_s \end{aligned} \tag{15}$$

Remark 1: It can be seen from Eq. (15) that the lumped uncertainty terms consist of approximation errors, state couplings, external disturbances, ground effect, and accelerations of the landing platform, which will be handled by the developed UDE-based controllers.

Then, the control problem is formulated as designing the effective position controllers to regulate the relative motion $\Delta\xi$ to track the smooth, continuous, and differentiable reference $\Delta\xi_r = [\,\Delta x_r \quad \Delta y_r \quad \Delta z_r\,]^T$, which specifies the landing trajectory of the quadrotor, in the presence of state couplings, random ship motion, ground effect, and external disturbances.

III. Control Design

This section presents the detailed derivation process of the UDE-based controller. To deal with random ship motion, the internal model principle is used to design the UDE filter based on the guidelines provided in [29]. The reference model is modified to ensure the tracking performance of the developed controller. The final forms of the controllers are also derived based on the developed UDE filter and reference model. The block diagram of the overall control system for the experimental platform is shown in Fig. 2, where $\Delta\psi$ and $\Delta\psi_r$ are the relative yaw and relative yaw reference, respectively. In the experiment, the heading of the quadrotor is controlled to be aligned with the heading of the landing platform using a simple proportional–integral (PI) controller, and the attitude control is achieved with the default attitude controllers in the Pixhawk flight controller. The UDE-based controllers are applied to control the relative altitude and relative horizontal positions.

A. Uncertainty and Disturbance Estimator-Based Controller

For clarity and simplicity, the details of developing the UDE-based controller for the relative altitude dynamics are provided here. Similar procedures can be followed for the relative horizontal dynamics [34]. Rewriting the relative altitude dynamics from Eq. (14) into the state-space form gives

$$\dot{\chi}_z = A_z \chi_z + B_z(u_z + D_z) \tag{16}$$

where

$$\chi_z = \begin{bmatrix} \Delta z \\ \Delta\dot{z} \end{bmatrix}$$

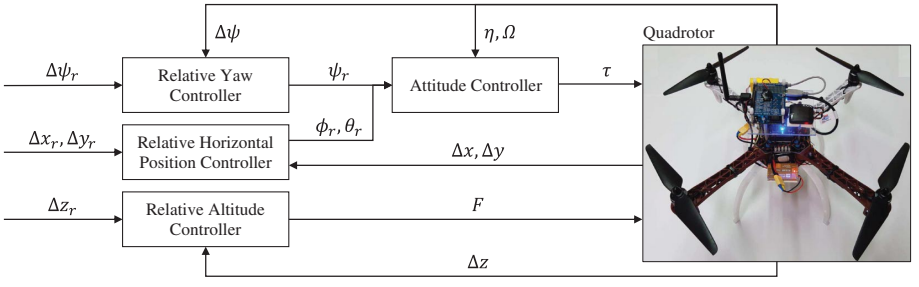

Fig. 2 Block diagram of the control structure.

is the state vector,

$$A_z = \begin{bmatrix} 0 & 1 \\ 0 & 0 \end{bmatrix}$$

is the state matrix, and

$$B_z = \begin{bmatrix} 0 \\ 1 \end{bmatrix}$$

is the input matrix. Design the stable reference model, which specifies the desired performance of the closed-loop system, as

$$\dot{\chi}_{mz} = A_{mz}\chi_{mz} + B_{mz}\chi_{zr} \tag{17}$$

where A_{mz} is the state matrix of the reference model, which should be designed as a Hurwitz matrix; B_{mz} is the input matrix of the reference model; χ_{mz} is the state vector of the reference model; and

$$\chi_{zr} = \begin{bmatrix} \Delta z_r \\ \Delta \dot{z}_r \end{bmatrix}$$

is a vector consisting of the reference and its first-order derivative. It should be noted that, in this work, the derivative of the reference ($\Delta \dot{z}_r$) is included in the reference model to enhance the tracking performance of the developed controller. The tracking error of the closed-loop system is defined as

$$e_z = \chi_{mz} - \chi_z \tag{18}$$

Taking the time derivative of Eq. (18) results in

$$\dot{e}_z = A_{mz}\chi_{mz} + B_{mz}\chi_{zr} - A_z\chi_z - B_z u_z - B_z D_z \tag{19}$$

The control objective is to drive the closed-loop system tracking error converging to zero with the desired closed-loop system error dynamics specified as

$$\dot{e}_z = A_{mz} e_z \tag{20}$$

Based on Eqs. (19) and (20), the control action term $B_z u_z$ is designed as

$$B_z u_z = A_{mz}\chi_z + B_{mz}\chi_{zr} - A_z\chi_z - B_z\hat{D}_z \tag{21}$$

where $B_z\hat{D}_z$ is the estimation of the lumped uncertainty term $B_z D_z$. The lumped uncertainty term $B_z D_z$ can be solved from the system dynamics [Eq. (16)] as

$$B_z D_z = \dot{\chi}_z - A_z\chi_z - B_z u_z \tag{22}$$

Following the procedures provided in [27], by adopting a stable proper filter $G_{fz}(s)$ that has unity gain and zero phase shift over the spectrum of the lumped uncertainty term, $B_z D_z$ can be accurately estimated as

$$B_z\hat{D}_z = \mathcal{L}^{-1}\{G_{fz}(s)\} * (\dot{\chi}_z - A_z\chi_z - B_z u_z) \tag{23}$$

where $*$ is the convolution operator, and $\mathcal{L}^{-1}\{\cdot\}$ is the inverse Laplace transform operator. Hence, the control action term [Eq. (21)] is rewritten as

$$B_z u_z = A_{mz}\chi_z + B_{mz}\chi_{zr} - A_z\chi_z - \mathcal{L}^{-1}\{G_{fz}(s)\} * (\dot{\chi}_z - A_z\chi_z - B_z u_z) \tag{24}$$

Solving for u_z results in the UDE-based control law

$$u_z = B_z^+\left[-A_z\chi_z + \mathcal{L}^{-1}\left\{\frac{1}{1-G_{fz}(s)}\right\} * (A_{mz}\chi_z + B_{mz}\chi_{zr}) - \mathcal{L}^{-1}\left\{\frac{sG_{fz}(s)}{1-G_{fz}(s)}\right\} * \chi_z\right] \tag{25}$$

where $B_z^+ = (B_z^T B_z)^{-1} B_z^T$ is the pseudoinverse of B_z.

B. Filter and Reference Model Design

According to the guidelines provided in [29], the filter is designed based on the internal model principle in the form of

$$G_{fz}(s) = 1 - \left(1 - \frac{f_{cz}}{s + f_{cz}}\right)\left(1 - \frac{2\zeta_z\omega_{0z}s}{s^2 + 2\zeta_z\omega_{0z}s + \omega_{0z}^2}\right) = \frac{(2\zeta_z\omega_{0z} + f_{cz})s^2 + 2\zeta_z\omega_{0z}f_{cz}s + f_{cz}\omega_{0z}^2}{s^3 + (2\zeta_z\omega_{0z} + f_{cz})s^2 + (2\zeta_z\omega_{0z}f_{cz} + \omega_{0z}^2)s + f_{cz}\omega_{0z}^2} \tag{26}$$

where $f_{cz}/(s + f_{cz})$ is a first-order low-pass filter with the cutoff frequency of f_{cz} to handle step disturbance; $2\zeta_z\omega_{0z}s/(s^2 + 2\zeta_z\omega_{0z}s + \omega_{0z}^2)$ is a second-order band-pass filter to handle sinusoidal disturbance with frequency ω_{0z}; and ζ_z denotes the damping ratio of the band-pass filter. The terms associated with the filter $G_{fz}(s)$ in Eq. (25) are calculated as

$$\frac{1}{1-G_{fz}(s)} = \frac{s^3 + (2\zeta_z\omega_{0z} + f_{cz})s^2 + (2\zeta_z\omega_{0z}f_{cz} + \omega_{0z}^2)s + f_{cz}\omega_{0z}^2}{s^3 + \omega_{0z}^2 s}$$

$$\frac{sG_{fz}(s)}{1-G_{fz}(s)} = \frac{(2\zeta_z\omega_{0z} + f_{cz})s^2 + 2\zeta_z\omega_{0z}f_{cz}s + f_{cz}\omega_{0z}^2}{s^2 + \omega_{0z}^2}$$

To ensure the reference model asymptotically tracking the descending command, which is a ramp signal in this work, the reference model is designed as

$$\dot{\chi}_{mz} = \begin{bmatrix} 0 & 1 \\ -\omega_{mz}^2 & -2\zeta_{mz}\omega_{mz} \end{bmatrix}\chi_{mz} + \begin{bmatrix} 0 & 0 \\ \omega_{mz}^2 & 2\zeta_{mz}\omega_{mz} \end{bmatrix}\begin{bmatrix} \Delta z_r \\ \Delta \dot{z}_r \end{bmatrix} \tag{27}$$

by incorporating the derivative of the reference signal, where ω_{mz} and ζ_{mz} are the parameters of the reference model. The final form of the relative altitude controller is simplified as

$$u_z = \mathcal{L}^{-1}\left\{\frac{1}{1-G_{fz}(s)}\right\} * (-\omega_{mz}^2\Delta z - 2\zeta_{mz}\omega_{mz}\Delta\dot{z} + \omega_{mz}^2\Delta z_r + 2\zeta_{mz}\omega_{mz}\Delta\dot{z}_r) - \mathcal{L}^{-1}\left\{\frac{sG_{fz}(s)}{1-G_{fz}(s)}\right\} * \Delta\dot{z} \tag{28}$$

During the landing process, the horizontal positions of the quadrotor are commanded in synchronization with the ship horizontal motions, which renders the constant relative position references. Thus, the reference models of the horizontal position dynamics are designed as

$$\dot{\chi}_{mx} = \begin{bmatrix} 0 & 1 \\ -\omega_{mx}^2 & -2\zeta_{mx}\omega_{mx} \end{bmatrix}\chi_{mx} + \begin{bmatrix} 0 & 0 \\ \omega_{mx}^2 & 0 \end{bmatrix}\begin{bmatrix} \Delta x_r \\ \Delta \dot{x}_r \end{bmatrix}$$

$$\dot{\chi}_{my} = \begin{bmatrix} 0 & 1 \\ -\omega_{my}^2 & -2\zeta_{my}\omega_{my} \end{bmatrix}\chi_{my} + \begin{bmatrix} 0 & 0 \\ \omega_{my}^2 & 0 \end{bmatrix}\begin{bmatrix} \Delta y_r \\ \Delta \dot{y}_r \end{bmatrix}$$

with the filters $G_{fx}(s)$ and $G_{fy}(s)$ chosen as

$$G_{fx}(s) = \frac{f_{cx}}{s + f_{cx}}$$

$$G_{fy}(s) = \frac{f_{cy}}{s + f_{cy}}$$

where ω_{mx}, ζ_{mx} and ω_{my}, ζ_{my} are the parameters of the reference models for the Δx and Δy dynamics, respectively, and f_{cx} and f_{cy} are the cutoff frequencies of the low-pass filters $G_{fx}(s)$ and $G_{fy}(s)$, respectively. Then, the final forms of the relative horizontal position controllers are given as

$$\begin{aligned} u_x &= \mathcal{L}^{-1}\left\{\frac{1}{1-G_{fx}(s)}\right\} * (-\omega_{mx}^2\Delta x - 2\zeta_{mx}\omega_{mx}\Delta\dot{x} + \omega_{mx}^2\Delta x_r) \\ &\quad - \mathcal{L}^{-1}\left\{\frac{sG_{fx}(s)}{1-G_{fx}(s)}\right\} * \Delta\dot{x} \\ u_y &= \mathcal{L}^{-1}\left\{\frac{1}{1-G_{fy}(s)}\right\} * (-\omega_{my}^2\Delta y - 2\zeta_{my}\omega_{my}\Delta\dot{y} + \omega_{my}^2\Delta y_r) \\ &\quad - \mathcal{L}^{-1}\left\{\frac{sG_{fy}(s)}{1-G_{fy}(s)}\right\} * \Delta\dot{y} \end{aligned} \tag{29}$$

IV. Stability Analysis

This section presents the detailed stability analysis of the closed-loop system. It is shown that, under the derived stability condition, the tracking errors of the closed-loop systems are bounded. Then, the asymptotic performance analysis of the reference model is provided.

A. Stability Analysis of the Closed-Loop System

Substituting Eq. (24) into the error dynamics [Eq. (19)] along with Eqs. (22) and (23) leads to the closed-loop system error dynamics

$$\dot{e}_z = A_{mz}e_z + \tilde{D}_z \tag{30}$$

where $\tilde{D}_z = \mathcal{L}^{-1}\{G_f(s) - 1\} * B_z D_z$ denotes the lumped uncertainty estimation error. Consider the following Lyapunov function candidate:

$$V(t) = e_z^T P e_z$$

where $P = P^T$ is a real symmetric positive-definite matrix. The time derivative of $V(t)$ is given by

$$\begin{aligned} \dot{V}(t) &= e_z^T P\dot{e}_z + \dot{e}_z^T P e_z \\ &= e_z^T P(A_{mz}e_z + \tilde{D}_z) + (e_z^T A_{mz}^T + \tilde{D}_z^T)Pe_z \\ &= e_z^T(PA_{mz} + A_{mz}^T P)e_z + 2e_z^T P\tilde{D}_z \\ &= -e_z^T Q e_z + 2e_z^T P\tilde{D}_z \end{aligned}$$

where Q is a positive-definite symmetric matrix defined by

$$PA_{mz} + A_{mz}^T P = -Q$$

Hence, it can be found that

$$\begin{aligned} \dot{V}(t) &\le -\lambda_{\min}(Q)\|e_z\|^2 + 2e_z^T P\tilde{D}_z \\ &\le -\lambda_{\min}(Q)\|e_z\|^2 + 2\lambda_{\max}(P)\|e_z\|\|\tilde{D}_z\| \end{aligned} \tag{31}$$

where $\lambda_{\min}(\cdot)$ and $\lambda_{\max}(\cdot)$ denote the minimum and maximum eigenvalues of a matrix, respectively. If the filter parameters, the reference model A_{mz}, and the matrix Q are chosen properly such that

$$\|\tilde{D}_z\| \le \frac{\lambda_{\min}(Q)}{2\lambda_{\max}(P)}\|e_z\|$$

then

$$\dot{V} \le 0 \tag{32}$$

Solving $e_z(t)$ from Eq. (30) results in

$$e_z(t) = \exp(A_{mz}t)e_z(0) + \int_0^t \exp[A_{mz}(t-\mu)]\tilde{D}_z(\mu)\,\mathrm{d}\mu \tag{33}$$

where $\exp(\cdot)$ is the exponential function. From Eq. (33), it could be seen that the condition

$$\|\tilde{D}_z\| \le \frac{\lambda_{\min}(Q)}{2\lambda_{\max}(P)}\|e_z\|$$

can be easily satisfied with the proper selection of the filter parameters, reference model A_{mz}, and matrix Q. Then, it can be concluded from Eq. (32) that

$$V(t) \le V(0) \le \gamma, \qquad \forall\ t \ge 0$$

where γ is the upper bound of the Lyapunov function candidate. Thus, for any bounded initial tracking error $e_z(0)$, $V(t) = e_z^T P e_z$ will remain bounded. Therefore, the closed-loop system tracking error e_z is also bounded from

$$\begin{aligned} V(t) &= e_z^T P e_z \\ &\ge \lambda_{\min}(P)\|e_z\|^2 \end{aligned}$$

Similar procedures can be followed to show that the closed-loop system tracking errors for the relative horizontal position dynamics, e_x and e_y, are bounded.

B. Performance Analysis of the Reference Model

Let χ_{mz1} be the first component of the vector χ_{mz}. Rewriting the reference model for the relative altitude controller [Eq. (27)] into the dynamics of χ_{mz1} and the command Δz_r leads to

$$\ddot{\chi}_{mz1} = -\omega_{mz}^2\chi_{mz1} - 2\zeta_{mz}\omega_{mz}\dot{\chi}_{mz1} + \omega_{mz}^2\Delta z_r + 2\zeta_{mz}\omega_{mz}\Delta\dot{z}_r \tag{34}$$

Taking the Laplace transform of Eq. (34) results in

$$X_{mz1}(s) = \frac{2\zeta_{mz}\omega_{mz}s + \omega_{mz}^2}{s^2 + 2\zeta_{mz}\omega_{mz}s + \omega_{mz}^2}\Delta Z_r(s)$$

where $X_{mz1}(s)$ and $\Delta Z_r(s)$ are the Laplace transform of $\chi_{mz1}(t)$ and $\Delta z_r(t)$, respectively. Define the tracking error of the reference model as

$$\begin{aligned} E_{mz}(s) &= \Delta Z_r(s) - X_{mz1}(s) \\ &= \frac{s^2}{s^2 + 2\zeta_{mz}\omega_{mz}s + \omega_{mz}^2}\Delta Z_r(s) \end{aligned} \tag{35}$$

The ramp reference signal during the descending phase is defined as $\Delta z_r(t) = z_{r0} + v_{zr}t$, where z_{r0} is the initial relative altitude reference during the hover phase, and v_{zr} is a constant that specifies the desired descending rate. Substituting $\Delta Z_r(s) = v_{zr}/s^2$ into Eq. (35) leads to

$$E_{mz}(s) = \frac{v_{zr}}{s^2 + 2\zeta_{mz}\omega_{mz}s + \omega_{mz}^2} \tag{36}$$

If the reference model parameters ω_{mz} and ζ_{mz} are properly chosen such that Eq. (36) is a stable proper transfer function, by applying the final value theorem to Eq. (36), there is

$$\begin{aligned} \lim_{t\to\infty} e_{mz}(t) &= \lim_{s\to 0} sE_{mz}(s) \\ &= \lim_{s\to 0}\frac{v_{zr}s}{s^2 + 2\zeta_{mz}\omega_{mz}s + \omega_{mz}^2} \\ &= 0 \end{aligned}$$

where $e_{mz}(t)$ is the inverse Laplace transform of $E_{mz}(s)$. Therefore, it can be concluded that $\chi_{mz1}(t)$ can asymptotically track the command signal $\Delta z_r(t)$.

V. Results and Discussion

In this section, the numerical simulations and experimental studies are carried out to validate the effectiveness of the developed UDE-based controllers. In the simulation, the sea state data and the ship RAO data from the literature [41,42] are used to accurately simulate the heave motion of a USS Joseph Hewes class destroyer under realistic sea condition. From the analysis of the derived ship heave acceleration spectrum and relative dynamics, a parameter selection guideline for ω_{0z} is provided to maximize the capability of the relative altitude controller. Extensive experimental studies are carried out to demonstrate that the quadrotor can successfully land on a three-dimensional moving landing platform under the influence of wind disturbance.

A. Numerical Simulation

The numerical simulation is performed using Matlab Simulink R2015b with the fixed-step solver, and the step size is 0.001 s. Because of the limited computational power of onboard microprocessors, it is noticed that the update rate of the horizontal position measurements from the camera can only reach 30 Hz. Furthermore, the relative altitude measurement update rate is set to 100 Hz in the experiment. Therefore, in the simulation, the sampling time is set to 0.033 s for the Δx and Δy measurement and 0.010 s for the Δz measurement. The quadrotor platform used in the simulation is a Hummingbird quadrotor from Ascending Technology [43]. The physical parameters of the quadrotor are listed in Table 1 [43,44]. The effect of the wind is simulated as disturbances d_x and d_y acting on the horizontal dynamics of the quadrotor. The details about the quadrotor model and wind disturbance calculation can be found in the Appendix.

1. *Ship Heave Motion Simulation with Sea State and Response Amplitude Operator Data*

The sea state 4 data of the North Atlantic from [42], which is tabulated in Table 2, are used to determine the parameters for the sea wave spectrum $S(\omega_w)$. It should be noticed that the percentage of probability of sea state 4 ranks the highest among all sea states. Let T_0 denote the modal wave period. The mean wave period can be calculated from the modal wave period as $T_1 = 0.772T_0$. Then, the RAO data in [41] corresponding to a USS Joseph Hewes class destroyer at an encounter angle of 150 deg and a forward speed of 10 kt are adopted for the calculation of the ship heave motion spectrum. The sea wave spectrum S and encounter wave spectrum S_E with the sea state 4 data are calculated and plotted in Fig. 3a. Figure 3b shows the ship heave motion spectrum S_R and ship heave acceleration spectrum S_{ACC}. The ship heave motion in seaway is simulated using Eq. (8) with $n = 1000$ and frequency ranging from 0.393 to 2 rad/s. The corresponding amplitude of the sinusoidal component (M_i), given the encounter frequency ω_{Ei}, is calculated using Eqs. (7) and (9) with the differential step of $\Delta\omega_E = 0.0016$ rad/s.

Remark 2: From the analysis of the relative dynamics [Eq. (14)] and lumped uncertainty terms [Eq. (15)], it is noticed that the random ship heave motion z_s creates problems for the accurate tracking of desired landing trajectory through ship heave acceleration $\ddot{z}_s$.

The ship heave acceleration is obtained from Eq. (8) in the form of

$$\ddot{z}_s(t) = \sum_{i=1}^{n} -\omega_{Ei}^2 M_i \sin(\omega_{Ei}t + \varphi_i)$$

The corresponding ship heave acceleration spectrum is obtained as

$$S_{\text{ACC}}(\omega_E) = \omega_E^4 S_R(\omega_E) \tag{37}$$

Let ω_{0R} and $\omega_{0\text{ACC}}$ denote the peak frequencies of the ship heave motion and ship heave acceleration spectrum, respectively, which have the highest power compared to other frequency components. From Fig. 3b, it is noticed that $\omega_{0R} = 0.8795$ rad/s and $\omega_{0\text{ACC}} = 1.0535$ rad/s are different.

Remark 3: Because the ship heave acceleration is included into the lumped uncertainty term, to maximally reduce the effect of the ship heave motion, the filter parameter ω_{0z} should be chosen as $\omega_{0\text{ACC}}$. This parameter selection guideline will be further validated using numerical simulation.

2. *Simulation Case 1: Landing on a Moving Ship at Sea State 4*

The objective of simulation case 1 is to let the quadrotor land on a three-dimensional moving ship at sea state 4 of the North Atlantic, which has an average wind speed of 19 kt (i.e., $v_{wd} = 9.774$ m/s), average significant wave height of 1.88 m, and most probable modal wave period of 8.8 s. The ship considered here is a USS Joseph Hewes class destroyer moving with a forward speed of 10 kt, which is 5.144 m/s. The ship is traveling in the positive $\boldsymbol{x}_I$ direction, and the encounter angle is 150 deg. The controller parameters for each degree of freedom (DOF) are listed in Table 3. The filter parameter ω_{0z} is set to 1.0535 rad/s, which is according to the peak of the ship heave acceleration spectrum shown in Fig. 3b. The landing process consists of three phases. The first phase is the lock-in phase, where the quadrotor is commanded to hover above the moving ship with the references given as $\Delta x_r = 0$ m, $\Delta y_r = 0$ m, and $\Delta z_r = -0.8$ m. After the synchronization between the quadrotor and the ship is achieved (i.e., the quadrotor could successfully hover above the ship), the second phase (descending) will be started by gradually reducing the relative altitude reference. From practical flight experience, it is noticed that the quadrotor will bounce up and down if directly commanded to land with the relative altitude reference reduced to zero. Therefore, when the quadrotor is close enough to the landing platform (i.e., less than 0.38 m), the final phase (touchdown) is initiated by decreasing the thrust at a constant rate. The simulation results are shown in Fig. 4, where x_r, y_r, and z_r are the calculated

Table 1 Quadrotor physical parameters used in simulation [43,44]

Parameter	Value
m	0.5 kg
I_{xx}	2.32×10^{-3} kg · m^2
I_{yy}	2.32×10^{-3} kg · m^2
I_{zz}	4.00×10^{-3} kg · m^2
l	0.175 m
k_M	1.5×10^{-9} (N · m)/rpm^2
k_F	6.11×10^{-9} N/rpm^2
k_m	20 s^{-1}
R	0.1016 m

Table 2 Annual sea state in North Atlantic [42]

		Sustained wind speed, kt		Significant wave height, m		Modal wave period, s	
Sea state number	Probability, %	Range	Mean	Range	Mean	Range	Most probable
2	6.80	7–10	8.5	0.1–0.5	0.3	3.3–12.8	7.5
3	23.70	11–16	13.5	0.5–1.25	0.88	5.0–14.8	7.5
4	27.80	17–21	19	1.25–2.5	1.88	6.1–15.2	8.8
5	20.64	22–27	24.5	2.5–4	3.25	8.3–15.5	9.7

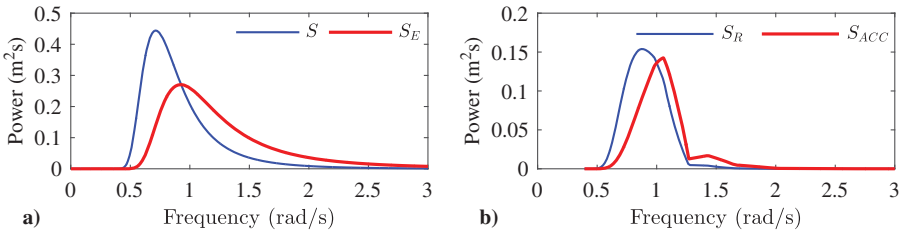

Fig. 3 Power spectrum.

Table 3 Controller parameters for simulation

DOF	ω_m	ζ_m	f_c	ω_0	ζ
Δz	0.9	1	260	1.0535	1
Δx	0.35	1	95	— —	— —
Δy	0.35	1	95	— —	— —

position references for the quadrotor in the inertia frame. Figures 4a, 4c, and 4e show the relative positions Δx, Δy, and Δz and their references Δx_r, Δy_r, and Δz_r, and Figs. 4b, 4d, and 4f present the quadrotor positions, x, y, and z, their references x_r, y_r, and z_r, and ship positions x_s, y_s, and z_s, in the inertia frame. The relative altitude Δz, relative altitude reference Δz_r, quadrotor altitude z, and its reference z_r in the inertia frame are negative because z_I, z_Q, and z_S are pointing downward. From the simulation results, it can be seen that the quadrotor can successfully land on the moving ship with the final landing accuracies (LAs) of 0.0284 m in the Δx direction and 0.0328 m in the Δy direction.

3. *Simulation Case 2: Effect of the Uncertainty and Disturbance Estimator Filter Parameter ω_{0z}*

The objective of the second simulation case is to evaluate the effect of different selections for the UDE filter parameter ω_{0z}. Different settings, $\omega_{0za} = 1.0535$ rad/s, $\omega_{0zb} = 0.8795$ rad/s, and $\omega_{0zc} = 1.2275$ rad/s, are considered under the same ship heave motion while keeping other controller parameters unchanged. It is intended to show that the tracking error of the relative altitude controller is maximally reduced with the parameter selection of $\omega_{0za} = \omega_{0\text{ACC}} = 1.0535$ rad/s, where $\omega_{0\text{ACC}}$ is the peak frequency of

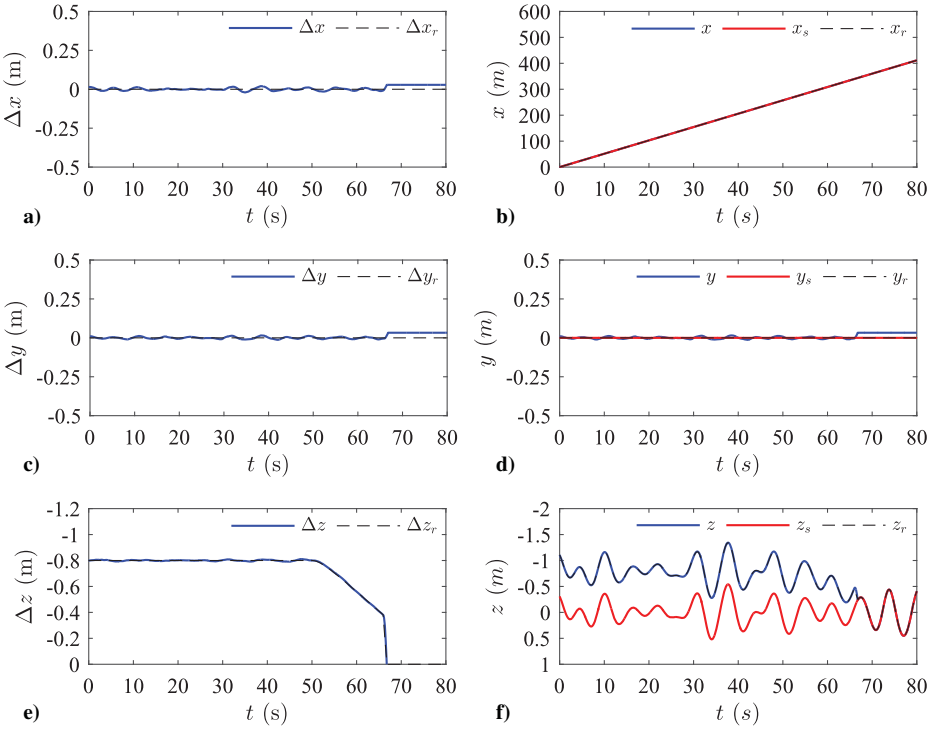

Fig. 4 Simulation case 1 results: landing on a moving ship at sea state 4.

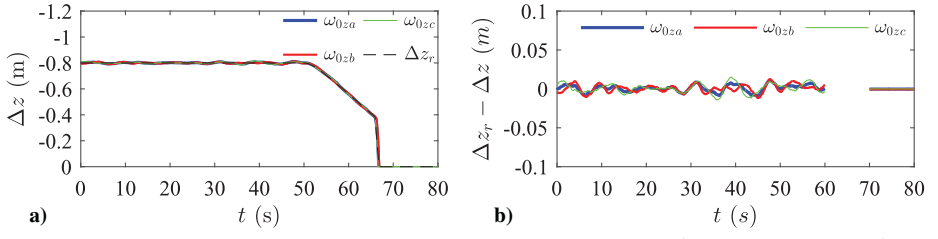

Fig. 5 Simulation case 2 results: effect of the UDE filter parameter ω_{0z}, where $\omega_{0za} = 1.0535$ rad/s, $\omega_{0zb} = 0.8795$ rad/s, and $\omega_{0zc} = 1.2275$ rad/s.

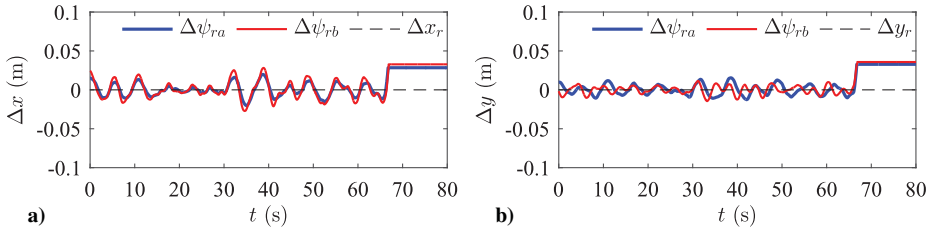

Fig. 6 Simulation case 3 results: effect of the relative yaw angle on landing accuracies, where $\Delta\psi_{ra} = 0$ deg and $\Delta\psi_{rb} = 30$ deg.

Table 4 Controller parameters for the nonlinear controller developed in [4]

DOF	k_P	k_I	k
Δz	10	10	10
Δx	10	5	— —
Δy	10	5	— —

the ship heave acceleration spectrum, which is shown in Fig. 3b. The results are shown in Fig. 5. Figures 5a and 5b show the relative altitudes and relative altitude tracking errors, respectively. The calculated root-mean-squared errors (RMSEs) are 0.0044 m for $\omega_{0_{za}}$, 0.0049 m for $\omega_{0_{zb}}$, and 0.0060 m for $\omega_{0_{zc}}$. From the simulation results, it can be seen that the tracking errors are maximally reduced when $\omega_{0_z} = \omega_{0\text{ACC}}$. The parameter selection guideline for ω_{0_z} is successfully validated.

4. Simulation Case 3: Effect of the Relative Yaw Angle on Landing Accuracies

The third simulation case is carried out to demonstrate the effect of the relative yaw on the final landing accuracies. Two different relative yaw references, $\Delta\psi_{ra} = 0$ deg and $\Delta\psi_{rb} = 30$ deg, are considered while keeping controller parameters unchanged. The simulation scenarios are the same as simulation case 1. Because the virtual

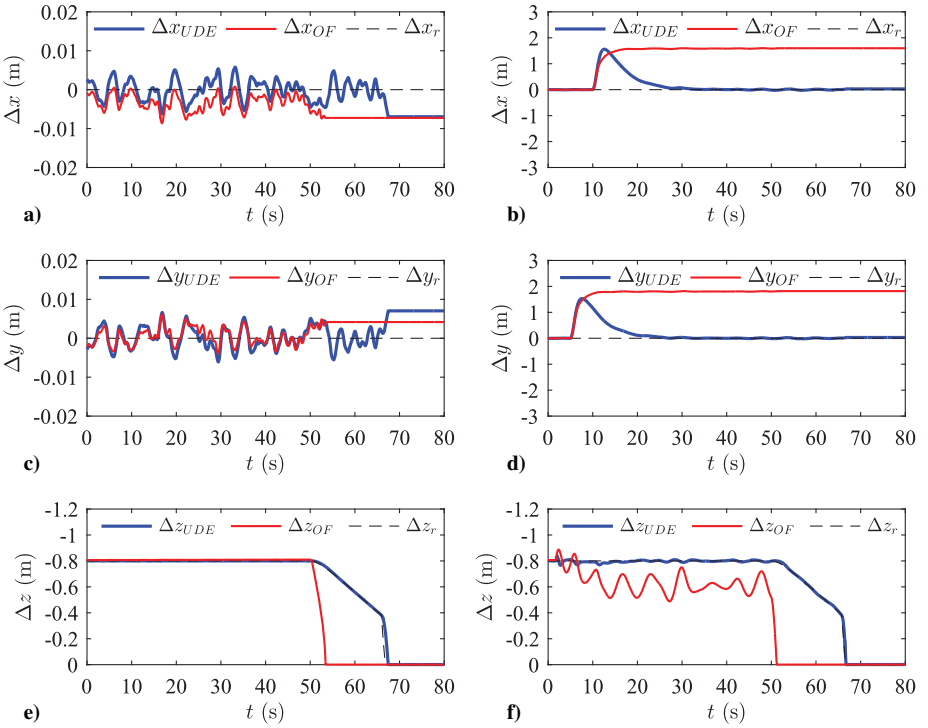

Fig. 7 Simulation case 4 results: comparison with the controller developed in [4].

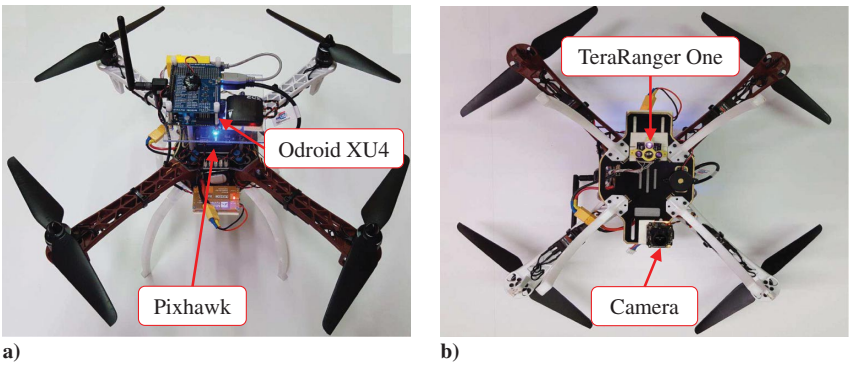

Fig. 8 Quadrotor platform for experimental validation: a) top view, and b) bottom view.

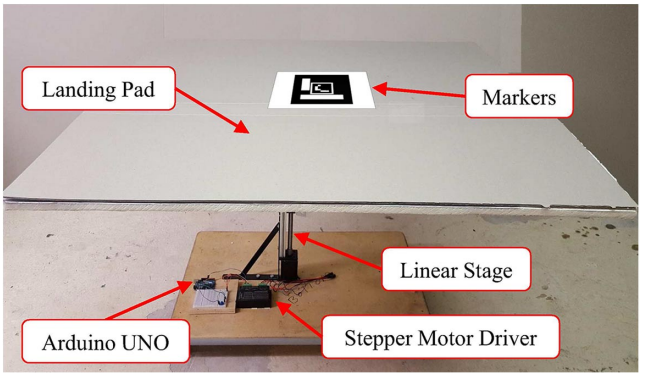

Fig. 9 Ship heave motion simulator.

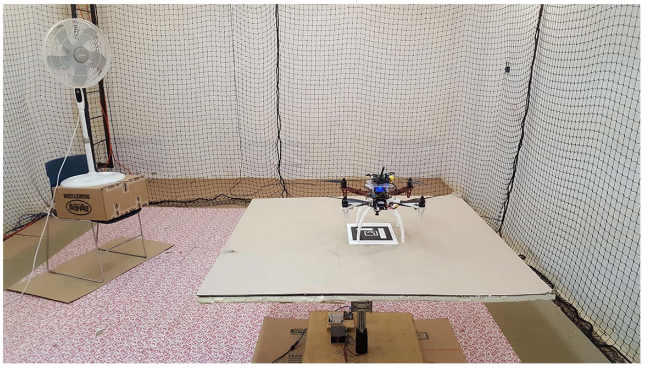

Fig. 11 Experimental field and setup.

control inputs for the quadrotor horizontal motions are designed based on assumption 3, it is intended to show that the relative yaw angle will affect the final landing accuracies. The results are shown in Fig. 6. Figures 6a and 6b show the relative horizontal positions Δx and Δy, respectively. It can be seen that the quadrotor can successfully land on the moving ship even with the nonzero relative yaw reference. The final LAs are 0.0284 m in the Δx direction and 0.0328 m in the Δy direction for $\Delta\psi_{ra} = 0$ deg as well as 0.0328 m in the Δx direction and 0.0358 m in the Δy direction for $\Delta\psi_{rb} = 30$ deg. It shows that the relative yaw angle has an effect on the final landing accuracies. More accurate landing is achieved when the quadrotor heading is controlled to align with the heading of the ship.

5. *Simulation Case 4: Comparison with the Existing Controller*

To demonstrate the advantages of the developed UDE-based controller, the comparative simulation study with the nonlinear optical flow controller proposed in [4] is carried out. In [4], a PI-type nonlinear controller is developed for stabilization of the hovering flight:

$$u = k_P w + k_I \int_0^t w \, \mathrm{d}\tau + mgz_I \tag{38}$$

where u are the control inputs of the position dynamics, k_P and k_I are the positive controller parameters, and $w = -(\Delta\dot{\xi}/\Delta z)$ represents the inertial average optical flow. In the landing process, Eq. (38) is used to control the horizontal dynamics, whereas the relative height is controlled using the landing controller in the form of

$$u_z = mk(w_z - w_z^d) + mg \tag{39}$$

where $w_z = -(\Delta\dot{z}/\Delta z)$ denotes the vertical component of the inertial average optical flow, and w_z^d is the desired value of w_z, which is set as 0.5. The control objective is to let the quadrotor autonomously land on the simulated ship with the same landing procedures described in simulation case 1. First, the nominal case is considered, where the ship is static and no wind disturbance is acting the quadrotor. The controller parameters of the developed UDE-based controller are the same as simulation case 1, which are shown in Table 3. The controller parameters for Eqs. (38) and (39) are listed in Table 4, which are chosen to have similar performance with the developed UDE-based controller in the nominal case for a fair comparison. Then, the disturbance rejection case is carried out with the same controller parameters, considering the ship heave motion and wind disturbance, which are the same as described in simulation case 1. The ship starts moving at around 2 s. Then, the wind disturbances are added to the $\boldsymbol{y}_Q$ direction at around 5 s and the $\boldsymbol{x}_Q$ direction at around 10 s, respectively. The simulation results are shown in Fig. 7, where Δx_{UDE}, Δy_{UDE}, and Δz_{UDE} denote the relative positions for the developed UDE-based controller, Δx_{OF}, Δy_{OF}, and Δz_{OF} represent the relative positions for the nonlinear optical flow controller developed in [4], and Δx_r, Δy_r, and Δz_r are the references for the developed UDE-based controller. Figures 7a, 7c, and 7e and Figs. 7b, 7d, and 7f show the simulation results for the nominal case and disturbance rejection case, respectively. From the simulation results, it could be seen that the nonlinear controller developed in [4] achieves faster landing, whereas the developed UDE-based controller outperforms in the disturbance rejection case. From Figs. 7b, 7d, and 7f, it is shown that the developed controller could successfully handle the disturbance and ship heave motion, whereas the nonlinear controller developed in [4] exhibits large errors. This simulation case has demonstrated the superiority and robustness of the developed UDE-based controller for handling external disturbances and ship heave motion.

Table 5 Controller parameters for experiments

DOF	ω_m	ζ_m	f_c	ω_0	ζ
Δz	0.6	1	260	1.0535	0.1
Δx	0.35	1	95	— —	— —
Δy	0.30	1	95	— —	— —

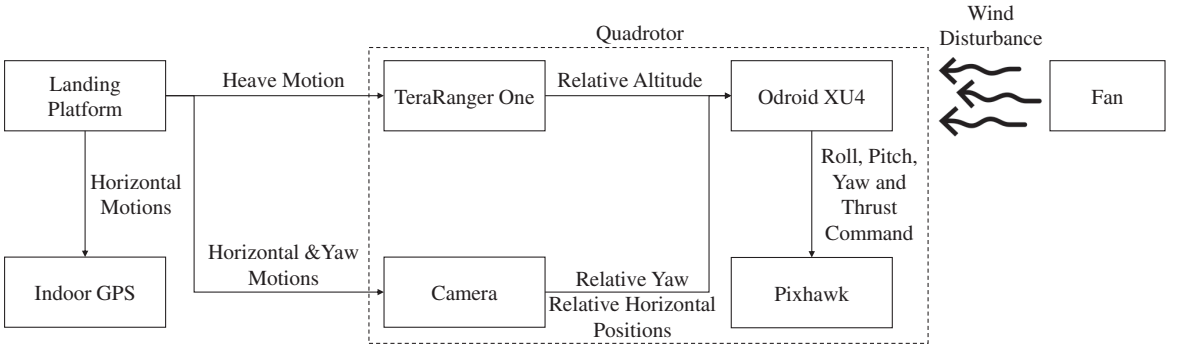

Fig. 10 Block diagram of the experimental setup.

B. Experimental Validation

1. Experimental Platforms and Setup

The experimental quadrotor platform is a self-built quadrotor, which is shown in Fig. 8.

The main flight control board is a Pixhawk flight controller, which runs the low-level attitude controllers. A companion computer Odroid XU4 is integrated to handle sensor data reading, image processing, and controller implementation. It contains two quad-core processors running Linux Ubuntu 14.04 and Robot Operating System Indigo. A TeraRanger One distance sensor is added to provide the relative height measurement, and an mvBlueFOX-MLC camera is added for the marker detection, which is achieved with the ArUco library [18] with the output of the marker positions and orientations. The thrust, roll, pitch, and yaw commands are sent to the Pixhawk from Odroid XU4 through serial communication. The self-built landing platform is shown in Fig. 9. Two markers with different sizes, whose side lengths are 18 cm and 5 cm, respectively, are attached to the center of the landing pad to ensure the availability of the localization information during the whole landing process. Though the ArUco marker-based navigation method provides six degrees of freedom motion information, the relative yaw and the relative horizontal positions are used for the control purpose. A linear stage is used to generate the heave motion of the landing pad. The horizontal motions of the landing platform are driven by hand pulling, which are

Table 6 Horizontal LAs and RMSEs of the experimental results

	DOF				
	Δz, m	Δx, m		Δy, m	
Case	RMSE	RMSE	LA	RMSE	LA
1	0.018	0.037	−0.041	0.060	−0.039
2	0.019	0.048	0.117	0.054	−0.103
3	0.019	0.059	0.036	0.072	0.065
4	0.021	0.055	−0.157	0.105	0.130

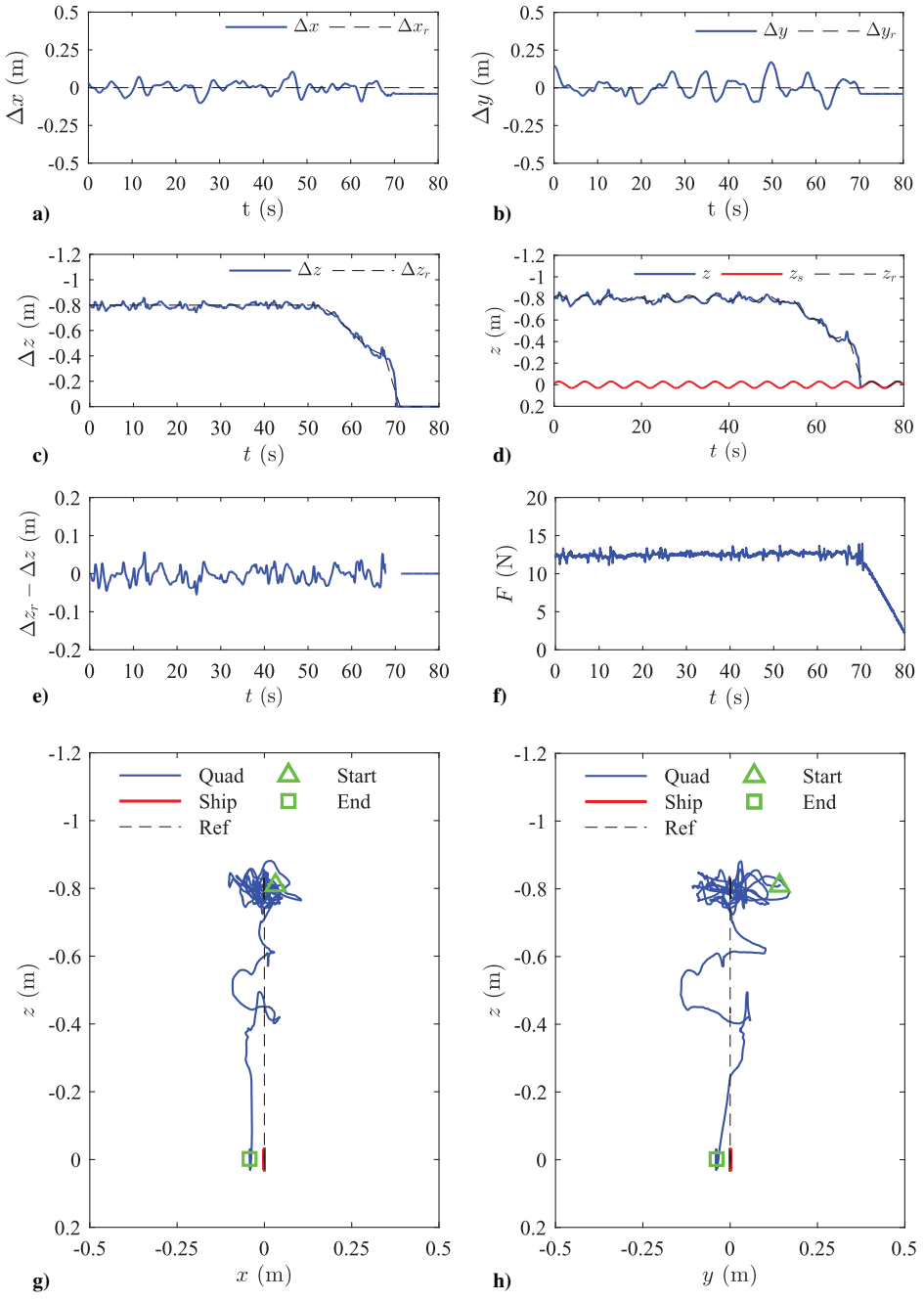

Fig. 12 Experimental case 1 results: landing on a vertically moving platform.

recorded using an indoor GPS system from Marvelmind Robotics [45]. The wind disturbance is generated by a fan. The block diagram that presents the overview of the experimental setup is shown in Fig. 10. Furthermore, the experimental field and setup are shown in Fig. 11.

Remark 4: In the experiment, the heave motion is simulated only as one sinusoidal signal because of the limited computational power of the microcontroller used for controlling the linear stage. Moreover, because of the limited space of the experimental field, the initial relative altitude of the quadrotor is chosen as $\Delta z_r = -0.8$ m, and the horizontal motions of the landing platform are generated by moving it back and forth within the experimental field to ensure the safe operation of the quadrotor.

2. *Experimental Case 1: Landing on a Vertically Moving Platform*

The objective of this experiment is to let the quadrotor autonomously land onto a vertically heaving platform. The selections of the controller parameters are listed in Table 5. The heave motion is simulated as one sinusoidal wave, $z_s(t) = 0.03\sin(1.0535t)$ m, whose frequency is according to the peak of the ship heave acceleration spectrum shown in Fig. 3b. The corresponding amplitude is calculated from Eq. (9). The quadrotor is initially hovering above the landing platform with the relative position references given as $\Delta x_r = 0$, $\Delta y_r = 0$, and $\Delta z_r = -0.8$ m. After the landing command is given by the pilot, the quadrotor will gradually descend when the relative horizontal position tracking errors are within certain predefined bounds. The landing procedures are the same as described in simulation case 1. The experimental results are shown in Fig. 12, where Figs. 12a, 12b, and 12c show the relative positions Δx, Δy, and Δz and their references Δx_r, Δy_r, and Δz_r; Fig. 12d presents the quadrotor altitude z, its reference z_r, and landing platform altitude z_s in the inertia frame; Fig. 12e shows the relative altitude tracking error $\Delta z_r - \Delta z$; Fig. 12f shows the control input of the relative altitude controller F; and Figs. 12g and 12h present the $x - z$ and $y - z$ views of the landing trajectory in the inertia frame. In Figs. 12g and 12h, Quad represents the quadrotor positions, Ship means the landing platform positions, Ref denotes the quadrotor position references, and Start and End represent the quadrotor initial and final positions, respectively. It should be noted that, in Fig. 12e, the relative tracking error for the touchdown phase of the landing process is not shown due to the fact that the UDE-based controller is disabled during that period of time. Because only the relative height Δz is measurable, the vertical motion of the quadrotor in the inertia frame is calculated by adding the relative height Δz with the landing platform heave motion z_s, which is determined from the linear stage controller. From the experimental results, it is shown that the quadrotor can successfully land on the vertically heaving platform with the horizontal LAs of -0.041 m in the Δx direction and -0.039 m in the Δy direction. The RMSEs for the relative positions are listed in Table 6. The roll and pitch angles ϕ and θ as well as their references ϕ_r and θ_r, which are generated by the developed horizontal position controllers, are shown in Figs. 13a and 13c. The roll and pitch tracking errors $\phi_r - \phi$ and $\theta_r - \theta$ are shown in Figs. 13b and 13d. Figure 13e shows the relative yaw $\Delta\psi$ and its

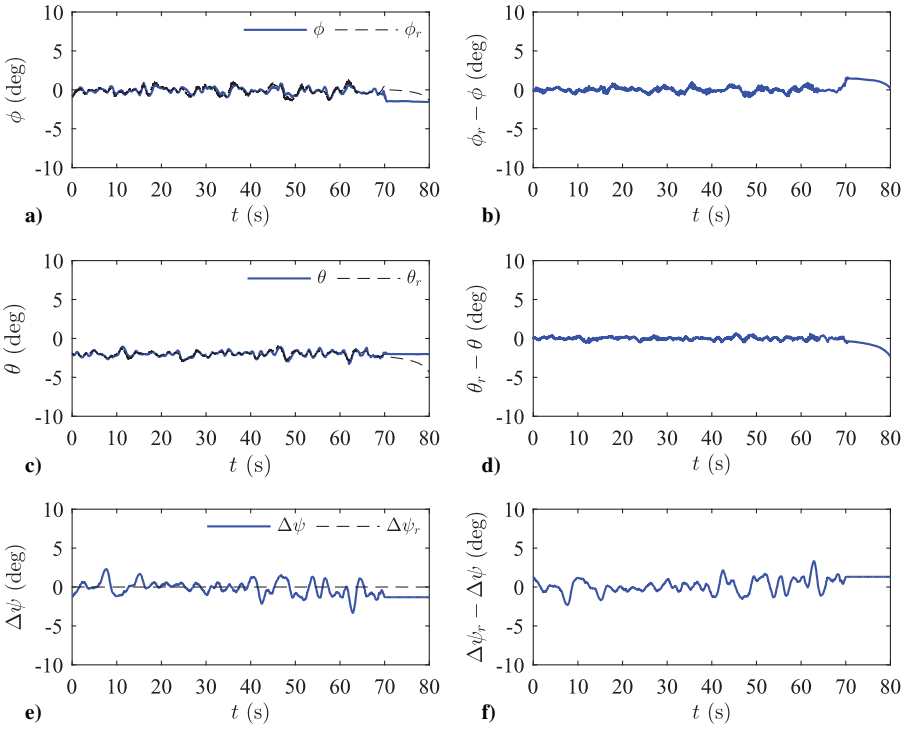

Fig. 13 Experimental case 1 results: landing on a vertically moving platform; attitude control performance.

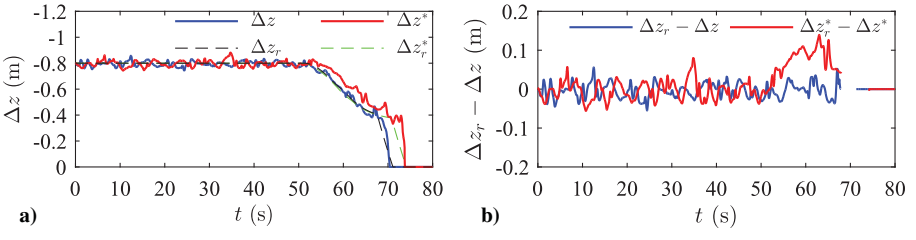

Fig. 14 Experimental case 1 results: landing on a vertically moving platform; comparison of the reference models.

reference $\Delta\psi_r$, and the relative yaw tracking error $\Delta\psi_r - \Delta\psi$ is shown in Fig 13f. From Fig. 13, it is shown that, although there exist tracking errors in the attitude controllers, good position control of the quadrotor is still achieved. Furthermore, it is demonstrated that the developed position controllers could be applied to the situation where the attitude tracking controllers are not perfect. Furthermore, it could be seen that the small-angle approximation used in designing ϕ_r and θ_r are successfully validated.

To demonstrate the superiority of the reference model design, the comparative experiments are carried out. The nominal reference model for a second-order system used in [27]

$$\dot{\chi}_{mz} = \begin{bmatrix} 0 & 1 \\ -\omega_{mz}^2 & -2\zeta_{mz}\omega_{mz} \end{bmatrix} \chi_{mz} + \begin{bmatrix} 0 \\ \omega_{mz}^2 \end{bmatrix} \Delta z_r^*$$

is implemented while keeping the controller parameters the same. In this work, to accurately track the landing trajectory, the reference model is modified by incorporating the derivatives of the reference signals. The experimental results are shown in Fig. 14, where Δz and Δz_r denote the measurement and reference signal for the modified reference model used in this work, respectively, and Δz^* and Δz_r^* are the measurement and reference signal for the nominal reference model used in [27], respectively. Figure 14a shows the relative altitudes Δz, and Fig. 14b presents the relative altitude tracking errors $\Delta z_r - \Delta z$. From the experimental results, it can be seen that both reference models perform similarly during hover phase. However, during descending phase, the nominal reference model cannot accurately track the command, whereas the modified reference model maintains good tracking performance. The reference trajectories are slightly varied due to the different initiating timing for the touchdown maneuver.

3. *Experimental Case 2: Landing on a Vertically Moving Platform with Wind Disturbance*

To test the robustness of the developed approach, the second case is carried out considering the external wind disturbance. The objective of

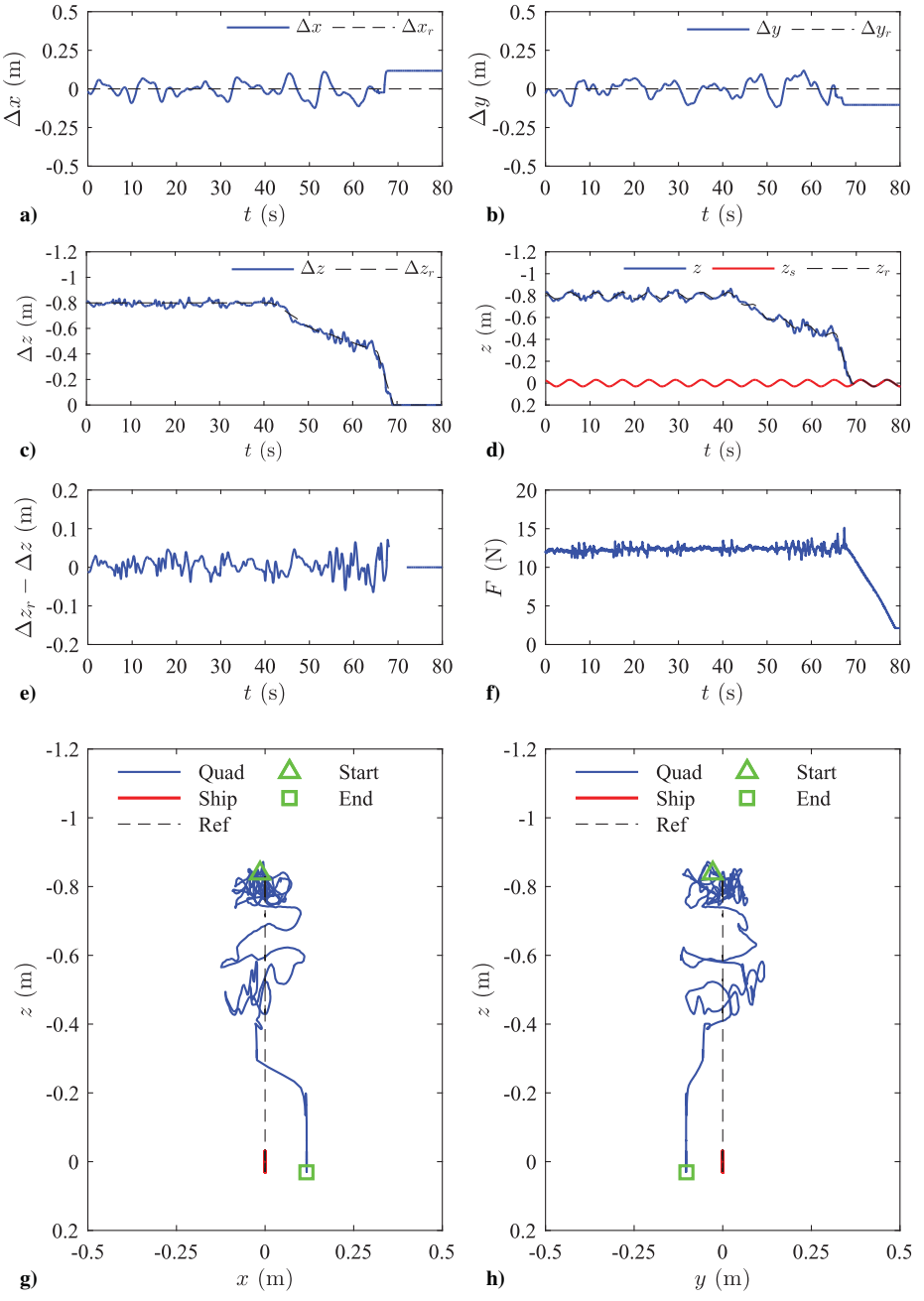

Fig. 15 Experimental case 2 results: landing on a vertically moving platform with wind disturbance.

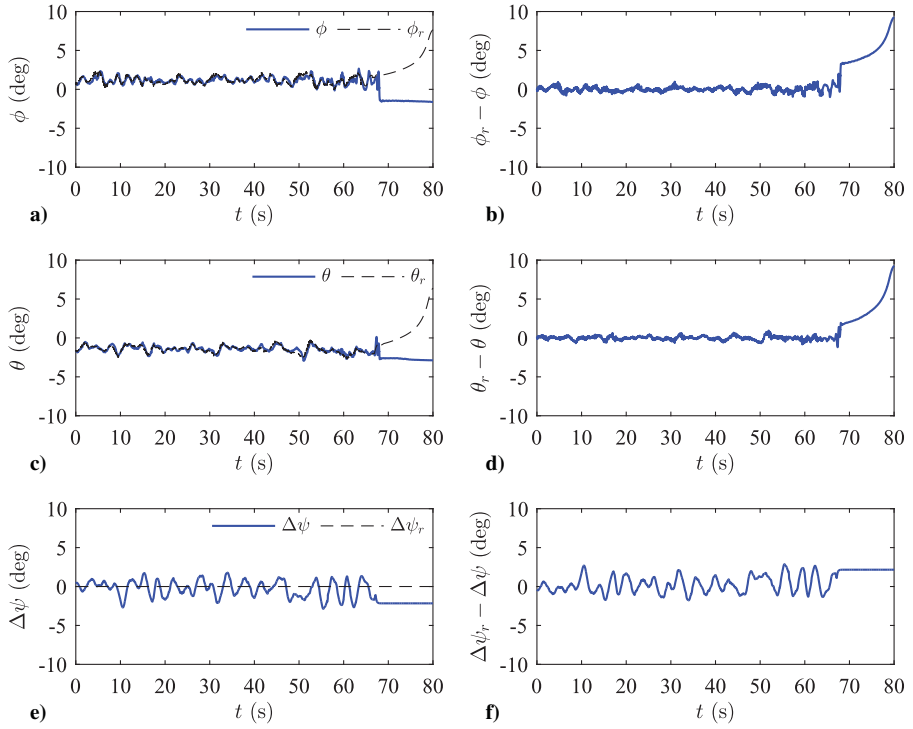

Fig. 16 Experimental case 2 results: landing on a vertically moving platform with wind disturbance; attitude control performance.

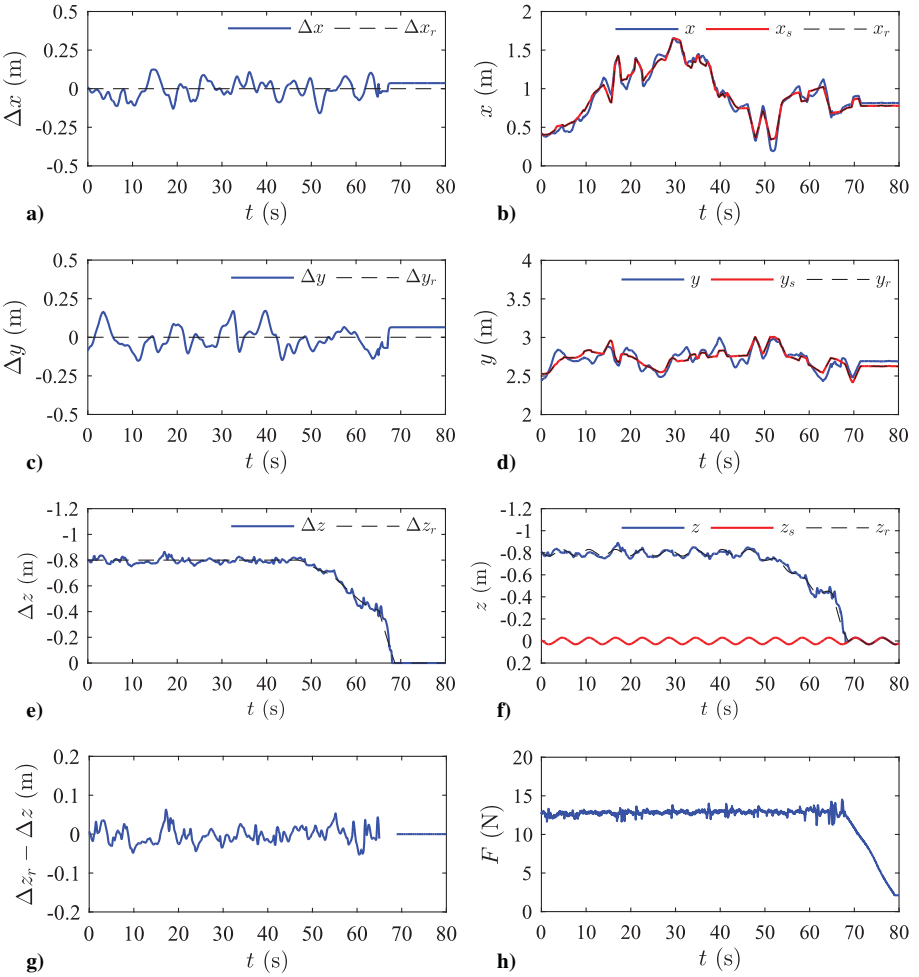

Fig. 17 Experimental case 3 results: landing on a three-dimensional moving platform.

this experiment is to let a quadrotor land on a vertically oscillating platform in the presence of an external disturbance. The wind disturbance is generated by a fan. The controller parameters and the heave motion generated are the same as experimental case 1. The relative position references are given as $\Delta x_r = 0$, $\Delta y_r = 0$, and $\Delta z_r = -0.8$ m for the initial lock-in phase. The same landing procedures as described in simulation case 1 are carried out. The experimental results are shown in Fig. 15, where Figs. 15a, 15b, and 15c show the relative positions Δx, Δy, and Δz and their references Δx_r, Δy_r, and Δz_r; Fig. 15d presents the quadrotor altitude z, its reference z_r, and landing platform altitude z_s in the inertia frame; Fig. 15e shows the relative altitude tracking error $\Delta z_r - \Delta z$; Fig. 15f shows the control input of the relative altitude controller F; and Figs. 15g and 15h present the $x - z$ and $y - z$ views of the landing trajectory in the inertia frame. In Figs. 15g and 15h, Quad represents the quadrotor positions, Ship means the landing platform positions, Ref denotes the quadrotor position references, and Start and End represent the quadrotor initial and final positions, respectively. It can be seen that autonomous landing is successfully achieved even under the influence of the wind disturbance. The final LAs are 0.117 m in the Δx direction and -0.103 m in the Δy direction, which is also shown in Table 6 along with the calculated relative position RMSEs. Figures 16a and 16c show the roll and pitch angles ϕ and θ and their references ϕ_r and θ_r. The roll and pitch tracking errors $\phi_r - \phi$ and $\theta_r - \theta$ are shown in Figs. 16b and 16d. Figure 16e shows the relative yaw $\Delta\psi$ and its reference $\Delta\psi_r$, and the relative yaw tracking error $\Delta\psi_r - \Delta\psi$ is shown in Fig. 16f.

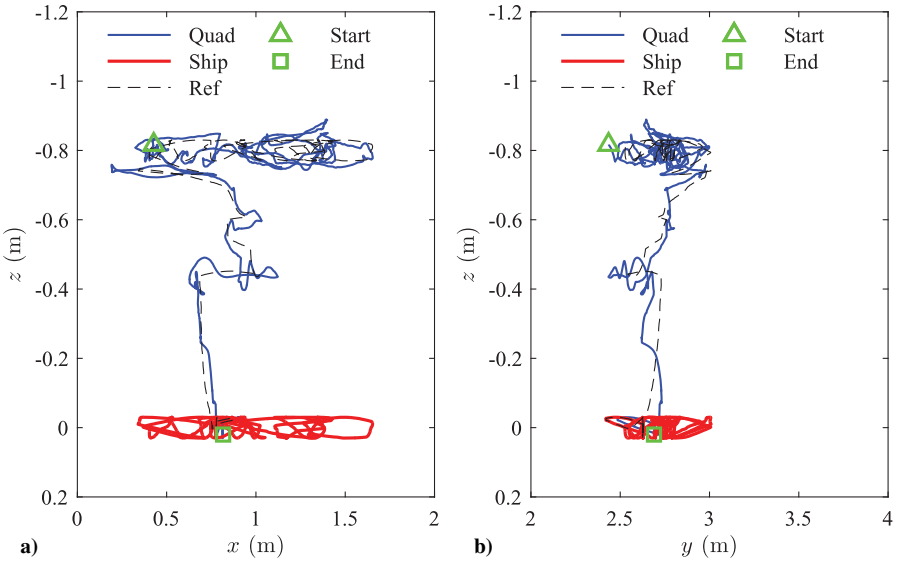

Fig. 18 Experimental case 3 results: landing on a three-dimensional moving platform.

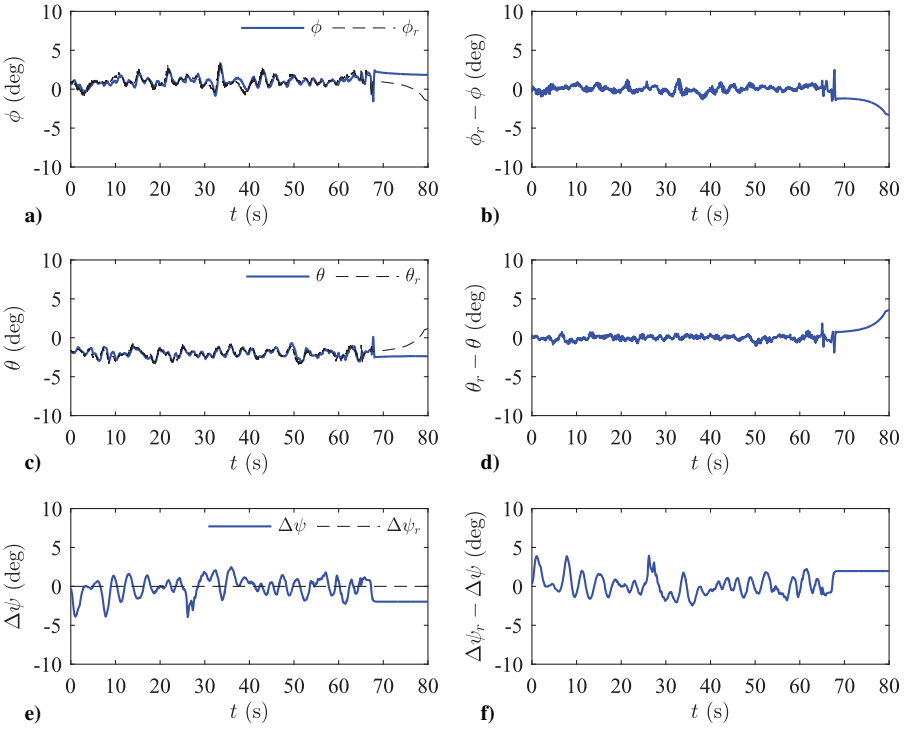

Fig. 19 Experimental case 3 results: landing on a three-dimensional moving platform; attitude control performance.

4. *Experimental Case 3: Landing on a Three-Dimensional Moving Platform*

To validate the tracking performance of the developed approach, experimental case 3 is carried out considering the three-dimensional motions of the landing platform. The objective of this experiment is to let the quadrotor autonomously land on a three-dimensional moving platform with solely relative measurements. The controller parameters and heave motion generated are the same as experimental case 1. The random horizontal motions of the landing platform are generated by hand pulling, which are recorded using an indoor GPS system from Marvelmind Robotics [45]. Then, the horizontal motions of the quadrotor in the inertia frame are calculated from the summation of the

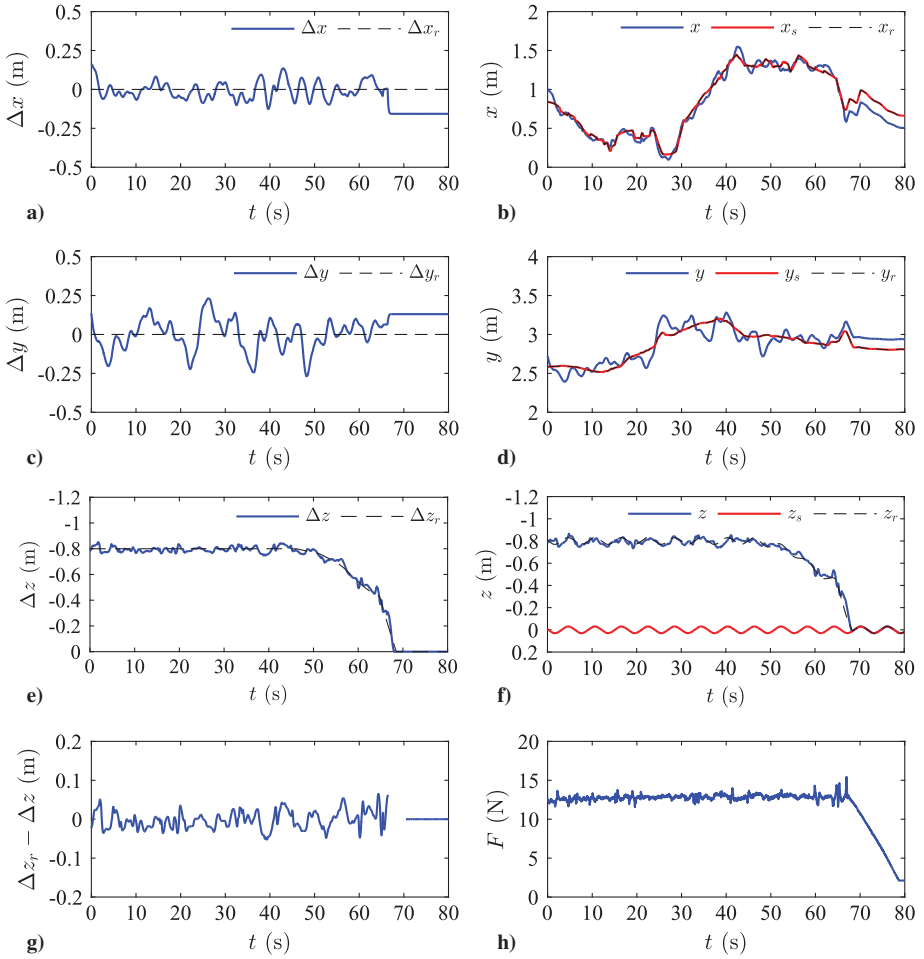

Fig. 20 Experimental case 4 results: landing on a three-dimensional moving platform with wind disturbance.

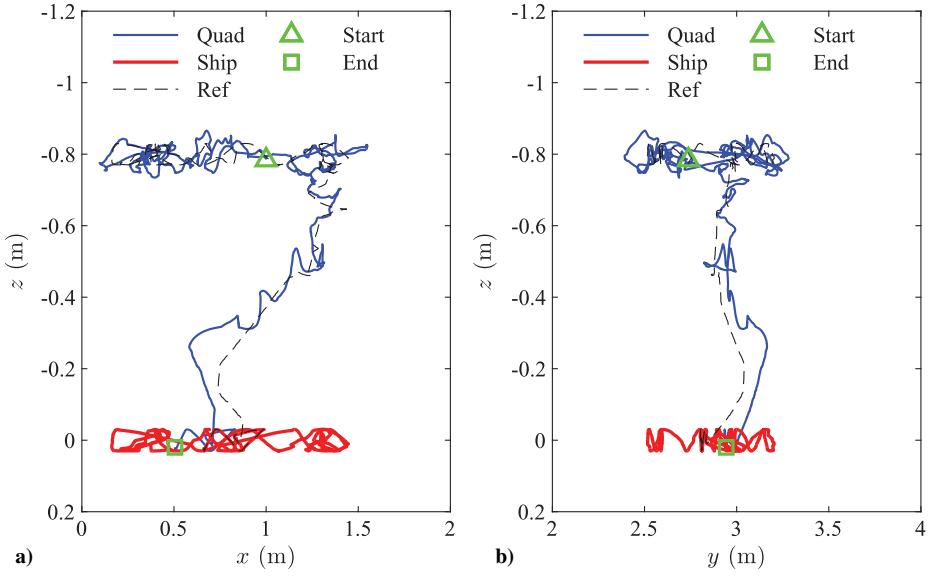

Fig. 21 Experimental case 4 results: landing on a three-dimensional moving platform with wind disturbance.

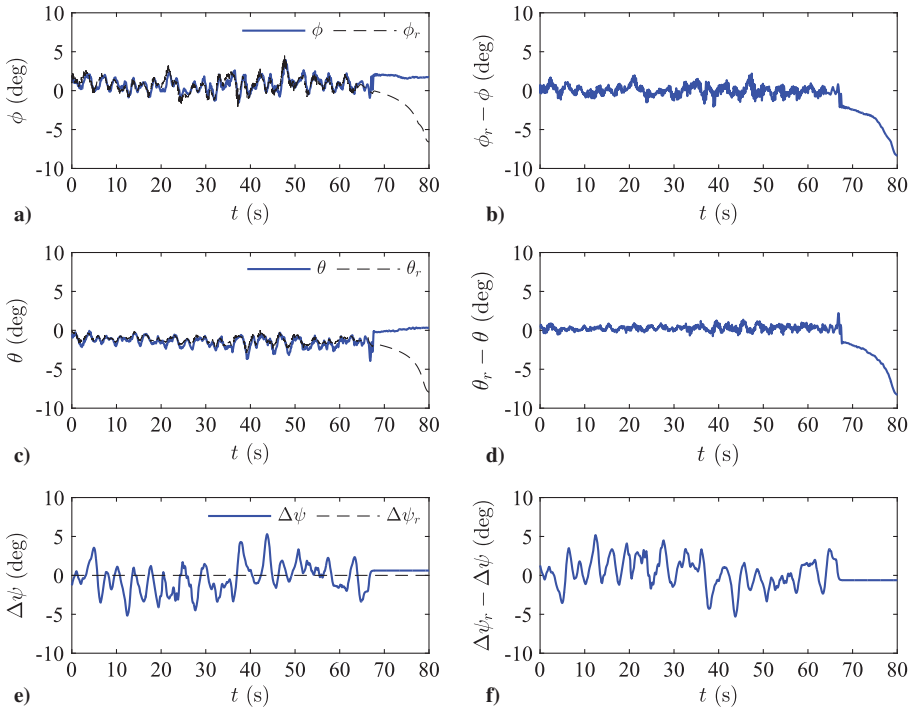

Fig. 22 Experimental case 4 results: landing on a three-dimensional moving platform with wind disturbance; attitude control performance.

relative motion Δx, Δy and the platform motion x_s, y_s. The quadrotor is initially hovering with relative position references of $\Delta x_r = 0$, $\Delta y_r = 0$, and $\Delta z_r = -0.8$ m. Then, autonomous landing is achieved with the same procedures described in simulation case 1 with the landing command given by the pilot. The experimental results are shown in Fig. 17, where Figs. 17a, 17c, and 17e show the relative positions Δx, Δy, and Δz and their references Δx_r, Δy_r, and Δz_r; Figs. 17b, 17d, and 17f present the quadrotor positions x, y, and z, their references x_r, y_r, and z_r, and landing platform positions x_s, y_s, and z_s in the inertia frame; Fig. 17g shows the relative altitude tracking error $\Delta z_r - \Delta z$; and Fig. 17h shows the control input of the relative altitude controller F. From the experimental results, it can be seen that the quadrotor successfully tracks the three-dimensional motions of the landing platform with the horizontal LAs of 0.036 m in the Δx direction and 0.065 m in the Δy direction. The horizontal LAs and the calculated position RMSEs are listed in Table 6. Figures 18a and 18b present the $x - z$ view and $y - z$ view of the landing trajectory in the inertia frame, respectively, where Quad represents the quadrotor positions, Ship means the landing platform positions, Ref denotes the quadrotor position references, and Start and End represent the quadrotor initial and final positions, respectively. Figures 19a and 19c show the roll and pitch angles ϕ and θ and their references ϕ_r and θ_r. The roll and pitch tracking errors $\phi_r - \phi$ and $\theta_r - \theta$ are shown in Figs. 19b and 19d. Figure 19e shows the relative yaw $\Delta\psi$ and its reference $\Delta\psi_r$, and the relative yaw tracking error $\Delta\psi_r - \Delta\psi$ is shown in Fig. 19f.

5. Experimental Case 4: Landing on a Three-Dimensional Moving Platform with Wind Disturbance

Experimental case 4 is carried out considering the three-dimensional motions of the landing platform and external wind disturbance. The objective of this experiment is to let the quadrotor land on a three-dimensional moving platform in the presence of wind disturbance. The controller parameters and heave motion generated are the same as experimental case 1. The random horizontal motions of the landing platform are generated by hand pulling, and the wind disturbance is generated using the fan shown in Fig. 11. The relative position commands are given as $\Delta x_r = 0$, $\Delta y_r = 0$, and $\Delta z_r = -0.8$ m for the initial hovering phase. The landing maneuver is initiated by the pilot with the landing procedures described in simulation case 1. The experimental results are shown in Fig. 20, where Figs. 20a, 20c, and 20e show the relative positions Δx, Δy, and Δz and their references Δx_r, Δy_r, and Δz_r; Figs. 20b, 20d, and 20f present the quadrotor positions x, y, and z, their references x_r, y_r, and z_r, and landing platform positions x_s, y_s, and z_s, in the inertia frame; Fig. 20g shows the relative altitude tracking error $\Delta z_r - \Delta z$; and Fig. 20h shows the control input of the relative altitude controller F. Even in the presence of the wind disturbance, the experimental results show that the quadrotor can still successfully track the random motion of the landing platform. Autonomous landing is achieved with the LAs of -0.157 m in the Δx direction and 0.130 m in the Δy direction, which is tabulated in Table 6 with the calculated relative position RMSEs. Figures 21a and 21b present the $x - z$ view and $y - z$ view of the landing trajectory in the inertia frame, respectively, where Quad represents the quadrotor positions, Ship means the landing platform positions, Ref denotes the quadrotor position references, and Start and End represent the quadrotor initial and final positions, respectively. Figures 22a and 22c show the roll and pitch angles ϕ and θ and their references ϕ_r and θ_r. The roll and pitch tracking errors $\phi_r - \phi$ and $\theta_r - \theta$ are shown in Figs. 22b and 22d. Figure 22e shows the relative yaw $\Delta\psi$ and its reference $\Delta\psi_r$, and the relative yaw tracking error $\Delta\psi_r - \Delta\psi$ is shown in Fig. 22f.

VI. Conclusions

This paper has presented the application of an uncertainty and disturbance estimator (UDE) based control approach to the autonomous shipboard landing control of a quadrotor unmanned aerial vehicle. The effectiveness of the developed method was validated through both numerical simulations and experimental studies, with various cases considered. The simulation and experimental results showed that the quadrotor successfully achieved autonomous landing on the three-dimensional moving platform even under the influence of external wind disturbances.

First, relative navigation was achieved with a distance sensor and a camera, which was used for marker detection. Then, the UDE-based controllers are developed in the relative coordinate with the UDE filter designed based on the internal model principle. The boundnesses of the closed-loop system tracking errors were shown with the stability analysis of the closed-loop system. In simulation studies, the ITTC spectrum, the sea state data, and the ship response amplitude operator data from the literature were used for the modeling of the ship motion in seaway. The effectiveness of the

parameter selection guideline based on the derived ship heave acceleration spectrum was successfully validated with simulation case 2 to achieve minimal tracking errors for relative altitude control. The comparative simulation with the nonlinear controller developed in [4] has demonstrated the superiority and robustness of the developed UDE-based controller for handling external disturbances and ship motion. The enhanced tracking performance of the modified reference model was shown with experimental case 1. It is of interest to investigate the application of the developed method to the tilting landing platform as a future research direction because the ship at sea also exhibits roll and pitch motions due to the wave excitation. Because the relative navigation method based on ArUco marker also provides the relative attitude information, it is possible to determine a time window when the quadrotor could safely land on the landing platform.

Appendix: Details of the Quadrotor Model and Wind Disturbance Calculation for Simulation

Let ω_k and ω_k^{cmd} be the kth motor speed and commanded kth motor speed, respectively, where $k = 1, \ldots, 4$ represent the motor number. The motor dynamics are modeled using first-order differential equations [44]:

$$\dot{\omega}_k = k_m(\omega_k^{\text{cmd}} - \omega_k)$$

where k_m denotes the bandwidth of the motor dynamics. The total thrust force and torques generated by four motors can be expressed as

$$\begin{bmatrix} F \\ \tau_\phi \\ \tau_\theta \\ \tau_\psi \end{bmatrix} = \begin{bmatrix} k_F & k_F & k_F & k_F \\ 0 & 0 & k_F l & -k_F l \\ k_F l & -k_F l & 0 & 0 \\ k_M & k_M & -k_M & -k_M \end{bmatrix} \begin{bmatrix} \omega_1^2 \\ \omega_2^2 \\ \omega_3^2 \\ \omega_4^2 \end{bmatrix} \tag{A1}$$

where l is the quadrotor arm length, k_F is the rotor thrust coefficient, and k_M is the rotor drag coefficient. It should be noted that Eq. (A1) represents the force and torque calculation for the Hummingbird quadrotor used in numerical simulation. The Hummingbird quadrotor is in the plus configuration, whereas the experimental platform is in the cross configuration.

Assumption 4: The wind direction is 225 deg with respect to the quadrotor heading. The disturbance magnitude is proportional to the square of the wind speed.

The disturbances are calculated as

$$d_x = d_y = \frac{\sqrt{2}}{2} K_{wd} v_{wd}^2$$

where v_{wd} denotes the wind speed, and $K_{wd} = 0.0470\ (\text{N} \cdot \text{s}^2)/\text{m}^2$ is the drag coefficient.

Acknowledgments

The authors would like to sincerely thank the editors and reviewers for their constructive comments, which have helped to greatly improve the quality of the paper.

References

[1] Hoffmann, G. M., Huang, H., Waslander, S. L., and Tomlin, C. J., "Quadrotor Helicopter Flight Dynamics and Control: Theory and Experiment," *AIAA Guidance, Navigation and Control Conference and Exhibit*, AIAA Paper 2007-6461, Aug. 2007. doi:10.2514/6.2007-6461

[2] Bayraktar, S., and Feron, E., "Experiments with Small Unmanned Helicopter Nose-Up Landings," *Journal of Guidance, Control, and Dynamics*, Vol. 32, No. 1, Jan. 2009, pp. 332–337. doi:10.2514/1.36470

[3] Watts, A. C., Ambrosia, V. G., and Hinkley, E. A., "Unmanned Aircraft Systems in Remote Sensing and Scientific Research: Classification and Considerations of Use," *Remote Sensing*, Vol. 4, No. 6, June 2012, pp. 1671–1692. doi:10.3390/rs4061671

[4] Herissé, B., Hamel, T., Mahony, R., and Russotto, F.-X., "Landing a VTOL Unmanned Aerial Vehicle on a Moving Platform Using Optical Flow," *IEEE Transactions on Robotics*, Vol. 28, No. 1, Feb. 2012, pp. 77–89. doi:10.1109/TRO.2011.2163435

[5] Kong, W., Zhou, D., Zhang, D., and Zhang, J., "Vision-Based Autonomous Landing System for Unmanned Aerial Vehicle: A Survey," *Proceedings of the International Conference on Multisensor Fusion and Information Integration for Intelligent Systems*, IEEE Publ., Piscataway, NJ, 2014, pp. 1–8. doi:10.1109/MFI.2014.6997750

[6] Kendoul, F., Lara, D., Fantoni, I., and Lozano, R., "Real-Time Nonlinear Embedded Control for an Autonomous Quadrotor Helicopter," *Journal of Guidance, Control, and Dynamics*, Vol. 30, No. 4, July 2007, pp. 1049–1061. doi:10.2514/1.27882

[7] Lanzon, A., Freddi, A., and Longhi, S., "Flight Control of a Quadrotor Vehicle Subsequent to a Rotor Failure," *Journal of Guidance, Control, and Dynamics*, Vol. 37, No. 2, March 2014, pp. 580–591. doi:10.2514/1.59869

[8] Gautam, A., Sujit, P., and Saripalli, S., "A Survey of Autonomous Landing Techniques for UAVs," *Proceedings of the International Conference on Unmanned Aircraft Systems*, IEEE Publ., Piscataway, NJ, 2014, pp. 1210–1218. doi:10.1109/ICUAS.2014.6842377

[9] "GPS Accuracy," National Coordination Office for Space-Based Positioning, Navigation, and Timing, Washington, D.C., http://www.gps.gov/systems/gps/performance/accuracy [retrieved 20 May 2017].

[10] Hardesty, M., Kennedy, S., Dixon, S., Berka, T., Graham, J., and Caldwell, D., "Development of Navigation and Automated Flight Control System Solutions for Maritime VTOL UAS Operations," Association for Unmanned Vehicle Systems International's Unmanned Systems North America (AUVSI), Las Vegas, NV, 2012, pp. 554–573.

[11] Garratt, M., Pota, H., Lambert, A., Eckersley-Maslin, S., and Farabet, C., "Visual Tracking and LIDAR Relative Positioning for Automated Launch and Recovery of an Unmanned Rotorcraft from Ships at Sea," *Naval Engineers Journal*, Vol. 121, No. 2, June 2009, pp. 99–110. doi:10.1111/nej.2009.121.issue-2

[12] Cao, Y., "UAV Circumnavigating an Unknown Target Under a GPS-Denied Environment with Range-Only Measurements," *Automatica*, Vol. 55, May 2015, pp. 150–158. doi:10.1016/j.automatica.2015.03.007

[13] Oh, S.-R., Pathak, K., Agrawal, S. K., Pota, H. R., and Garratt, M., "Approaches for a Tether-Guided Landing of an Autonomous Helicopter," *IEEE Transactions on Robotics*, Vol. 22, No. 3, June 2006, pp. 536–544. doi:10.1109/TRO.2006.870657

[14] Alarcon, F., Santamaria, D., and Viguria, A., "UAV Helicopter Relative State Estimation for Autonomous Landing on Moving Platforms in a GPS-Denied Scenario," *IFAC-PapersOnLine*, Vol. 48, No. 9, Sept. 2015, pp. 37–42. doi:10.1016/j.ifacol.2015.08.056

[15] Yakimenko, O. A., Kaminer, I. I., Lentz, W. J., and Ghyzel, P. A., "Unmanned Aircraft Navigation for Shipboard Landing Using Infrared Vision," *IEEE Transactions on Aerospace and Electronic Systems*, Vol. 38, No. 4, Oct. 2002, pp. 1181–1200. doi:10.1109/TAES.2002.1145742

[16] Yang, S., Ying, J., Lu, Y., and Li, Z., "Precise Quadrotor Autonomous Landing with SRUKF Vision Perception," *Proceedings of the International Conference on Robotics and Automation*, IEEE Publ., Piscataway, NJ, 2015, pp. 2196–2201. doi:10.1109/ICRA.2015.7139489

[17] Ling, K., "Precision Landing of a Quadrotor UAV on a Moving Target Using Low-Cost Sensors," M.S. Thesis, Univ. of Waterloo, Waterloo, ON, Canada, 2014.

[18] Garrido-Jurado, S., Munoz-Salinas, R., Madrid-Cuevas, F. J., and Marin-Jimenez, M. J., "Automatic Generation and Detection of Highly Reliable Fiducial Markers Under Occlusion," *Pattern Recognition*, Vol. 47, No. 6, June 2014, pp. 2280–2292. doi:10.1016/j.patcog.2014.01.005

[19] "TeraRanger," Terabee SAS, France, http://www.teraranger.com [retrieved 20 May 2017].

[20] Shin, H., You, D., and Shim, D. H., "Autonomous Shipboard Landing Algorithm for Unmanned Helicopters in Crosswind," *Journal of Intelligent & Robotic Systems*, Vol. 74, No. 1, April 2014,

pp. 347–361.
doi:10.1007/s10846-013-9927-2

[21] Tan, C. K., Wang, J., Paw, Y. C., and Liao, F., "Autonomous Ship Deck Landing of a Quadrotor Using Invariant Ellipsoid Method," *IEEE Transactions on Aerospace and Electronic Systems*, Vol. 52, No. 2, April 2016, pp. 891–903.
doi:10.1109/TAES.2015.140850

[22] Hu, B., Lu, L., and Mishra, S., "Fast, Safe and Precise Landing of a Quadrotor on an Oscillating Platform," *Proceedings of the American Control Conference*, IEEE Publ., Piscataway, NJ, 2015, pp. 3836–3841.
doi:10.1109/ACC.2015.7171928

[23] Chen, F., Jiang, R., Zhang, K., Jiang, B., and Tao, G., "Robust Backstepping Sliding-Mode Control and Observer-Based Fault Estimation for a Quadrotor UAV," *IEEE Transactions on Industrial Electronics*, Vol. 63, No. 8, Aug. 2016, pp. 4899–4908.
doi:10.1109/TIE.2016.2547365

[24] Marconi, L., Isidori, A., and Serrani, A., "Autonomous Vertical Landing on an Oscillating Platform: An Internal-Model Based Approach," *Automatica*, Vol. 38, No. 1, Jan. 2002, pp. 21–32.
doi:10.1016/S0005-1098(01)00184-4

[25] Yang, X., Garratt, M., and Pota, H., "Monotonous Trend Estimation of Deck Displacement for Automatic Landing of Rotorcraft UAVs," *Journal of Intelligent and Robotic Systems*, Vol. 61, No. 1, Jan. 2011, pp. 267–285.
doi:10.1007/s10846-010-9474-z

[26] Serra, P., Cunha, R., Hamel, T., Cabecinhas, D., and Silvestre, C., "Landing of a Quadrotor on a Moving Target Using Dynamic Image-Based Visual Servo Control," *IEEE Transactions on Robotics*, Vol. 32, No. 6, Dec. 2016, pp. 1524–1535.
doi:10.1109/TRO.2016.2604495

[27] Zhong, Q.-C., and Rees, D., "Control of Uncertain LTI Systems Based on an Uncertainty and Disturbance Estimator," *ASME Journal of Dynamic Systems, Measurement, and Control*, Vol. 126, No. 4, Dec. 2004, pp. 905–910.
doi:10.1115/1.1850529

[28] Ren, B., Zhong, Q.-C., and Chen, J., "Robust Control for a Class of Non-Affine Nonlinear Systems Based on the Uncertainty and Disturbance Estimator," *IEEE Transactions on Industrial Electronics*, Vol. 62, No. 9, Sept. 2015, pp. 5881–5888.
doi:10.1109/TIE.2015.2421884

[29] Ren, B., Zhong, Q.-C., and Dai, J., "Asymptotic Reference Tracking and Disturbance Rejection of UDE-Based Robust Control," *IEEE Transactions on Industrial Electronics*, Vol. 64, No. 4, April 2017, pp. 3166–3176.
doi:10.1109/TIE.2016.2633473

[30] Ren, B., Wang, Y., and Zhong, Q.-C., "UDE-Based Control of Variable-Speed Wind Turbine Systems," *International Journal of Control*, Vol. 90, No. 1, Jan. 2017, pp. 121–136.
doi:10.1080/00207179.2015.1126678

[31] Wang, Y., Ren, B., and Zhong, Q.-C., "Robust Power Flow Control of Grid-Connected Inverters," *IEEE Transactions on Industrial Electronics*, Vol. 63, No. 11, Nov. 2016, pp. 6887–6897.
doi:10.1109/TIE.2016.2586439

[32] Zhong, Q. C., Wang, Y., and Ren, B., "UDE-Based Robust Droop Control of Inverters in Parallel Operation," *IEEE Transactions on Industrial Electronics*, Vol. 64, No. 9, Sept. 2017, pp. 7552–7562.
doi:10.1109/TIE.2017.2677309

[33] Dai, J., Lu, Q., Ren, B., and Zhong, Q.-C., "Robust Attitude Tracking Control for a Quadrotor Based on the Uncertainty and Disturbance Estimator," *Proceedings of the Dynamic Systems and Control Conference*, American Soc. of Mechanical Engineers, New York, 2015, Paper V001T06A004.
doi:10.1115/DSCC2015-9900

[34] Lu, Q., Ren, B., Parameswaran, S., and Zhong, Q.-C., "Robust Position Control of a Quadrotor Using Onboard Optical Flow Sensor," *Dynamic Systems and Control Conference*, American Soc. of Mechanical Engineers, New York, 2016, Paper V001T05A002.
doi:10.1115/DSCC2016-9812

[35] Lu, Q., Ren, B., Parameswaran, S., and Zhong, Q.-C., "Uncertainty and Disturbance Estimator-Based Robust Trajectory Tracking Control for a Quadrotor in a Global Positioning System-Denied Environment," *ASME Journal of Dynamic Systems, Measurement, and Control*, Vol. 140, No. 3, March 2018, Paper 031001.
doi:10.1115/1.4037736

[36] Cheeseman, I. C., and Bennett, W. E., "The Effect of Ground on a Helicopter Rotor in Forward Flight," TR 3021, Aeronautical Research Council, London, 1955.

[37] Yoo, C. S., Park, B. J., Cho, A., and Kang, Y. S., "Simulation Based on Motion Platform for Tilt Rotor UAV Shipboard Landing," *Proceedings of the International Conference on Control, Automation and Systems*, IEEE Publ., Piscataway, NJ, 2015, pp. 1747–1750.
doi:10.1109/ICCAS.2015.7364647

[38] Hervas, J. R., Reyhanoglu, M., and Tang, H., "Automatic Landing Control of Unmanned Aerial Vehicles on Moving Platforms," *Proceedings of the International Symposium on Industrial Electronics*, IEEE Publ., Piscataway, NJ, 2014, pp. 69–74.
doi:10.1109/ISIE.2014.6864588

[39] Michel, W. H., "Sea Spectra Revisited," *Marine Technology*, Vol. 36, No. 4, Jan. 1999, pp. 211–227.

[40] Perez, T., and Blanke, M., "Simulation of Ship Motion in Seaway," Tech. Rept. EE02037, Dept. of Electrical and Computer Engineering, Univ. of Newcastle, Newcastle, Australia, 2002.

[41] Applebee, T., and Baitis, A., "Response Amplitude Operator Predictions for the USS BELKNAP (DLG-26) and USS JOSEPH HEWES (DE-1052) Class Destroyers," TR SPD-590-01, Naval Ship Research and Development Center, Bethesda, Maryland, 1974.

[42] Faltinsen, O. M., *Sea Loads on Ships and Offshore Structures*, Cambridge Univ. Press, Cambridge, U.K., 1993, p. 32.

[43] "Ascending Technologies," Intel Deutschland GmbH, Krailling, Deutschland, http://www.asctec.de/en [retrieved 20 May 2017].

[44] Powers, C., Mellinger, D., and Kumar, V., "Quadrotor Kinematics and Dynamics," *Handbook of Unmanned Aerial Vehicles*, edited by K. Valavanis, and G. Vachtsevanos, Springer, Dordrecht, 2015, pp. 307–328.
doi:10.1007/978-90-481-9707-1_71.

[45] *Marvelmind Robotics*, Marvelmind Inc., Sunnyvale CA, http://www.marvelmind.com [retrieved 20 May 2017].